Biogeosciences Discuss., 8, 3537–3618, 2011
www.biogeosciences-discuss.net/8/3537/2011/
doi:10.5194/bgd-8-3537-2011


Biogeosciences Discussions



# Nitrogen transfers and air-sea $N_2O$ fluxes in the upwelling off Namibia within the oxygen minimum zone: a 3-D model approach

**E. Gutknecht[1], I. Dadou[1], B. Le Vu[1], G. Cambon[1], J. Sudre[1], V. Garçon[1], E. Machu[2], T. Rixen[3], A. Kock[4], A. Flohr[3], A. Paulmier[1,5], and G. Lavik[6]**

[1]Laboratoire d'Etudes en Géophysique et Océanographie Spatiales (UMR 5566, CNRS/CNES/UPS/IRD), Toulouse, France
[2]Laboratoire de Physique des Océans (UMR 6523, CNRS/Ifremer/IRD/UBO), Plouzané, France
[3]Leibniz Center for Tropical Marine Ecology, Bremen, Germany
[4]Leibniz-Institut for Marine Science – Marine Biogeochemistry, Kiel, Germany
[5]Instituto del Mar del Peru, Esquina Gamarra y General Valle S/N chucuito Callao, Lima, Peru
[6]Max Plank Institut for Marine Microbiology, Bremen, Germany







Received: 25 February 2011 – Accepted: 22 March 2011 – Published: 4 April 2011

Correspondence to: E. Gutknecht (elodie.gutknecht@legos.obs-mip.fr)

Published by Copernicus Publications on behalf of the European Geosciences Union.





BGD
8, 3537–3618, 2011



## Abstract

As regions of high primary production and being often associated to Oxygen Minimum Zones (OMZs), Eastern Boundary Upwelling Systems (EBUS) represent key regions for the oceanic nitrogen (N) cycle. Indeed, by exporting the Organic Matter (OM) and nutrients produced in the coastal region to the open ocean, EBUS can play an important role in sustaining primary production in subtropical gyres. Losses of fixed inorganic N, through denitrification and anammox processes and through nitrous oxide ($N_2O$) emissions to the atmosphere, take place in oxygen depleted environments such as EBUS, and alleviate the role of these regions as a source of N. In the present study, we developed a 3-D coupled physical/biogeochemical (ROMS/BioBUS) model for investigating the full N budget in the Namibian sub-system of the Benguela Upwelling System (BUS). The different state variables of a climatological experiment have been compared to different data sets (satellite and in situ observations) and show that the model is able to represent this biogeochemical oceanic region.

The N transfer is investigated in the Namibian upwelling system using this coupled model, especially in the Walvis Bay area between 22° S and 24° S where the OMZ is well developed ($O_2 < 0.5\,\mathrm{ml\,O_2\,l^{-1}}$). The upwelling process advects $24.2 \times 10^{10}\,\mathrm{mol\,N\,yr^{-1}}$ of nitrate enriched waters over the first 100 m over the slope and over the continental shelf. The meridional advection by the alongshore Benguela current brings also nutrient-rich waters with $21.1 \times 10^{10}\,\mathrm{mol\,N\,yr^{-1}}$. $10.5 \times 10^{10}\,\mathrm{mol\,N\,yr^{-1}}$ of OM are exported outside of the continental shelf (between 0 and 100-m depth). 32.4% and 18.1% of this OM are exported by advection in the form of Dissolved and Particulate Organic Matters (DOM and POM), respectively, however vertical sinking of POM represents the main contributor (49.5%) to OM export outside of the first 100-m depth of the water column on the continental shelf. The continental slope also represents a net N export ($11.1 \times 10^{10}\,\mathrm{mol\,N\,yr^{-1}}$) between 0 and 100-m depth: advection processes export 14.4% of DOM and 1.8% of POM, and vertical sinking of POM contributes to 83.8%. Between 100 and 600-m depth, water column denitrification and





BGD
8, 3537–3618, 2011



anammox constitute a fixed inorganic N loss of $2.2 \times 10^8$ mol N $yr^{-1}$ on the continental shelf and slope, which will not significantly influence the N transfer from the coast to the open ocean. At the bottom, an important quantity of OM is sequestrated in the upper sediments of the Walvis Bay area. 78.8% of POM vertical sinking at 100-m depth is sequestrated on the shelf sediment. Only 14% of POM vertical sinking reaches the sediment on the slope without being remineralized.

From our estimation, the Walvis Bay area (0–100 m), can be a substantial N source ($28.7 \times 10^{10}$ mol N $yr^{-1}$) for the eastern part of the South Atlantic Subtropical Gyre. Assuming the same area for the South Atlantic Subtropical Gyre as the North Atlantic Subtropical Gyre, this estimation is equivalent to $3.7 \times 10^{-2}$ mol N $m^{-2}$ $yr^{-1}$ for the Walvis Bay area, and 0.38 mol N $m^{-2}$ $yr^{-1}$ by extrapolating for the entire Benguela upwelling system. This last estimation is of the same order as other possible N sources sustaining primary production in the subtropical gyres.

The continental shelf off Walvis Bay area does not represent more than 1.2% of the world's major eastern boundary regions and 0.006% of the global ocean, its estimated $N_2O$ emission ($2.9 \times 10^8$ mol $N_2O$ $yr^{-1}$), using a parameterization based on oxygen consumption, contributes to 4% of the emissions in the eastern boundary regions, and represents 0.2% of global ocean $N_2O$ emission. Hence, even if the Walvis Bay area is a small domain, its $N_2O$ emissions have to be taken into account in the atmospheric $N_2O$ budget.

## 1 Introduction

Uncertainties remain on the nutrient sources sustaining primary production in the subtropical gyres of the ocean. Several processes could be at work (Charria et al., 2008a): (1) transport of nutrients by mesoscale activity; (2) Ekman transport of Dissolved Organic Matter (DOM) originated from the enriched borders of the subtropical gyre and which is slowly remineralized; (3) biological fixation of nitrogen gas ($N_2$) at the ocean-atmosphere interface; (4) atmospheric transport and deposition of reactive nitrogen





BGD
8, 3537–3618, 2011



(N); (5) and transport of nutrients and Organic Matter (OM) from the coastal upwelling areas. Eastern Boundary Upwelling Systems (EBUS) could be a source of N, especially on the eastern border of the subtropical gyres, but also in remote locations since for example OM produced in the Canary upwelling system could irrigate the North Atlantic Ocean (Pelegrí et al., 2006). Indeed, although EBUS do not cover a large surface of the global ocean (0.3%), their productivity is among the highest in the ocean and represents about 2% of the primary production (Quiñones, 2010 for a review) and 11% of the new primary production of the global ocean (Chavez and Toggweiler, 1995). However, EBUS are often associated with Oxygen Minimum Zones (OMZs), the main regions of oceanic fixed inorganic N loss (e.g. Codispoti et al., 2001; Paulmier and Ruiz-Pino, 2009) which could mitigate the N source effect to the subtropical gyre.

Among the different EBUS (California, Humboldt, Canary and Benguela), the Benguela upwelling system (BUS) in the South Atlantic Ocean plays a special role. The BUS presents one of the highest primary production of all EBUS (Carr, 2002; Carr and Kearns, 2003; Chavez and Messie, 2009). It is the only one bordered by two warm currents: in the northern part, the Angola current enriched in nutrients and poor in oxygen content (Monteiro et al., 2006; Mohrholz et al., 2008), and in the southern part, the Agulhas current with its leakage of anticyclonic and cyclonic eddies carrying warm nutrient depleted and cold nutrient enriched waters, respectively (Boebel et al., 2003; Lutjeharms et al., 2003; Richardson et al., 2003; Schmid et al., 2003). As for the other EBUS, the trade winds maintain a horizontal pressure gradient along the coast associated to a coastal geostrophic current towards the equator: the Benguela current with cold and nutrient enriched waters. This EBUS is characterized by high levels of eddy kinetic energy reflecting the intense mesoscale activity which takes place under the form of eddies, filaments, fronts and Rossby waves (e.g., Penven et al., 2001; Charria et al., 2006; Capet et al., 2008; Veitch et al., 2009; Gutknecht et al., 2010) as well as in other EBUS.

Due to its high productivity and subsequent export production, an intense remineralization occurs between 100 and 600-m depth in the northern part of the BUS,





BGD
8, 3537–3618, 2011



especially in the Namibian upwelling region between 20° S and 25° S (Monteiro et al., 2006; Hutchings et al., 2009). In this depth range, the oxygen content of the Namibian upwelling area presents a specific OMZ centered on the wide (Western Africa) shelf. Suboxic concentrations below 0.5 ml $O_2$ $l^{-1}$ and even below the detection limit during some periods of the year are encountered in Walvis Bay (Monteiro et al., 2006, 2008). During these anoxic events, in addition to the respiratory barrier that affects zooplankton and fish (Ekau et al., 2010), sulfur emissions can occur with subsequent impacts on the mortality of commercial species (benthic communities such as demersal fish, lobster and shellfish). The BUS OMZ is controlled by local productivity and stratification while its variability is mainly controlled by remote forcing related to the low oxygen content of the poleward Angola current (Monteiro et al., 2008, 2011). In this OMZ, denitrification and anammox occur and induce massive fixed inorganic N loss (Kuypers et al., 2005; Lavik et al., 2009), reaching more than 1 Tg N $yr^{-1}$ (Kuypers et al., 2005) and hence could alleviate the role of N source for the South Atlantic Subtropical Gyre.

Furthermore, the OMZs in the EBUS are usually associated with carbon dioxide ($CO_2$) (Paulmier et al., 2011) and nitrous oxide ($N_2O$) (Codispoti et al., 2001; Cornejo et al., 2006; Farias et al., 2007) productions inducing coupled ($CO_2$ and $N_2O$) or decoupled ($CO_2$ or $N_2O$) emissions from the ocean to the atmosphere (Paulmier et al., 2008). $N_2O$ is a greenhouse gas ~300 times more efficient than $CO_2$ (Jain et al., 2000; Ramaswamy et al., 2001) and its present increase in the atmosphere plays a key role on the stratospheric ozone and tropospheric heat budget (IPCC; Denman et al., 2007). The ocean is a major source of $N_2O$ contributing about 30% of the atmospheric $N_2O$ budget (Bange, 2006; Denman et al., 2007). Coastal upwellings, where OMZ processes affecting the $N_2O$ cycle occur (denitrification and mainly nitrification), could contribute up to 50% of the oceanic source (Nevison et al., 2003).

Over the last years, OMZs have expanded due to stronger stratification of the ocean and weaker ocean ventilation (Stramma et al., 2008, 2010), this phenomenon being more critical in the coastal areas than in the open ocean (Gilbert et al., 2010), especially for the EBUS. The OMZs intensification and expansion currently observed in the





BGD
8, 3537–3618, 2011



EBUS (Stramma et al., 2008, 2010) might result in a considerable increase in oceanic fixed inorganic N losses and $N_2O$ emissions to the atmosphere (Codispoti et al., 2001; Codispoti, 2010; Naqvi et al., 2010).

In our study of the Namibian upwelling system, the following questions are addressed: (1) what is the significance of the N transfer from the coast to the eastern part of the South Atlantic Subtropical Gyre as compared to the other N sources for the open ocean? (2) What is the loss of fixed inorganic N via denitrification/anammox? And (3) what is the oceanic $N_2O$ production?

To answer these questions, an approach based on coupled modeling, and in-situ and satellite data is followed. A biogeochemical model representing the N cycle, one of the main limiting nutrients in the ocean, and the processes related to OMZ has been developed and coupled to the 3-D hydrodynamical model over the Namibian upwelling system. This coupled model and the data used are presented in Sects. 2 and 3, respectively. The evaluation of the model performance is presented using different statistical metrics in Sect. 4. Then, a N budget in the Walvis Bay area (between 22° S and 24° S) is presented in Sect. 5.

## 2 Coupled physical/biogeochemical model

### 2.1 Hydrodynamical model: ROMS

The hydrodynamical model used in this study is the Regional Ocean Modeling System (ROMS; Shchepetkin and McWilliams, 2003, 2005), in its version with the 2-way nesting capability (ROMS-AGRIF; Penven et al., 2006a; Debreu et al., 2011). This model is briefly described in this section. It is a split-explicit and free-surface model that considers the Boussinesq and hydrostatic assumptions when solving the primitive equations. The model is discretized in the vertical on a sigma or topography-following stretched coordinate system. Explicit lateral viscosity is zero everywhere in the modeled domain, except in sponge layer at open boundaries where it increases smoothly on several





BGD
8, 3537–3618, 2011



grid points. It uses an adaptative open boundary conditions combining outward radiations and nudging towards prescribed external boundary conditions (Marchesiello et al., 2001). The vertical turbulent closure is parameterized using the KPP boundary layer schemes (Large et al., 1994).

Recently, a ROMS-AGRIF nested configuration of South Africa region (SAfE for South African Experiment) has been developed by Penven et al. (2006b) and Veitch et al. (2009). It is a two nested grid AGRIF configuration, consisting in a 1/4° coarse grid covering Indian, Austral and Atlantic regions around South Africa, extending from 2.5° W to 54.75° E and from 4.8° S to 46.75° S (SAfE Coarse Resolution configuration (SAfE CR), hereafter referred to SAfE "parent" domain in Fig. 1) including and "feeding" a 1/12° finer grid covering the Northern and Southern BUS, extending from 3.9° E to 19.8° E and from 12.1° S to 35.6° S (SAfE High Resolution configuration (SAfE HR), hereafter referred to SAfE "child" domain in Fig. 1). These two SAfE configurations (SAfE CR and HR) have been validated, in particular the SAfE HR one for the BUS (Veitch et al., 2009). Considering that, we used the SAfE HR outputs to provide the initial and open boundary conditions of the Namibian configuration developed here (see Sect. 2.3; small domain in red in Fig. 1).

### 2.2 Biogeochemical model: BioBUS

The hydrodynamical model ROMS is coupled to a **Bio**geochemical model developed for the **B**enguela **U**pwelling **S**ystem, named **BioBUS**. The evolution of a biological tracer concentration $C_i$ is determined by an advective-diffusive equation:

$$\frac{\partial C_i}{\partial t} = -\nabla\cdot(\boldsymbol{u}C_i) + A_\rho\nabla^2 C_i + \frac{\partial}{\partial z}(K_P\frac{\partial C_i}{\partial z}) + \mathrm{SMS}(C_i) \quad (1)$$

The advection (with $\boldsymbol{u}$ the velocity vector) is represented by the first term on the right-hand side, the horizontal diffusion (with $A_\rho$ the horizontal eddy diffusion coefficient) by the second term, and the vertical mixing (with turbulent diffusion coefficient $K_P$) by the third term. The last term represents the "Source-Minus-Sink" term (SMS) due to biological activity.





BGD
8, 3537–3618, 2011



BioBUS (Fig. 2) is a nitrogen-based model derived from a $N_2P_2Z_2D_2$ model (Koné et al., 2005), which has been successfully used to simulate the first trophic levels of the Benguela ecosystem. It takes into account the main planktonic communities and their specificities in the Benguela upwelling ecosystem. In this model, nitrate and ammonium represent the pool of dissolved inorganic N. Phytoplankton and zooplankton are split into small (flagellates and ciliates, respectively) and large (diatoms and copepods, respectively) organisms. Detritus are also separated into small and large particulate compartments. We added a Dissolved Organic Nitrogen (DON) compartment. Indeed, DOM is an important reservoir of OM and plays an important role in supplying nitrogen or carbon from the coastal region to the open ocean (Huret et al., 2005). The simulated DON is the semi-labile one as the refractory and labile pools of DON have too long (hundred of years) and too short (less than a day) turnover rates, respectively (Kirchman et al., 1993; Carlson and Ducklow, 1995). The BioBUS model also includes nitrite to have a more detailed description of the microbial loop: ammonification/nitrification processes under oxic conditions, and denitrification/anammox processes under anoxic conditions (Yakushev et al., 2007). These processes are oxygen-dependent, so an oxygen equation has been introduced in the BioBUS model. To complete this nitrogen-based model, $N_2O$ was introduced using the Nevison et al. (2003) parameterization which allows to determine the $N_2O$ production in function of the oxygen amount consumed by nitrification and the depth.

Interactions between the different compartments of the BioBUS model are summarized in Fig. 2. All state variables (Table 1) are expressed in mmol $m^{-3}$. The formulation of the SMS terms for each of the biogeochemical tracers is given in Appendix A. Parameter values are given in Table 2.

Due to different modifications and additions made from the original biogeochemical model of Koné et al. (2005), we had to adapt the BioBUS model, especially some of the parameter values within the range of parameter values found in the literature (Table 2). Indeed, parameters linked to the microbial loop (hydrolysis of detritus $\mu_{D_S}$ and $\mu_{D_L}$, mineralization rate of particulate organic matter $K_{NP4}$ and dissolved organic





BGD
8, 3537–3618, 2011



matter $K_{ND4}$ from Yakushev et al. (2007) formulations, sinking velocity of large detritus $w_{D_L}$) were adjusted in order to better represent the distribution of nutrients and oxygen from the coast to the open ocean. Also, as a more detailed representation of the nitrification was introduced in the BioBUS model as compared to Koné et al. (2005), some of the parameter values associated with nutrients uptake by the phytoplankton (half saturation constants $K_{NO_{3_{P_S}}}$ and $K_{NH_{4_{P_L}}}$) had to be adjusted in order to obtain a better agreement for the chlorophyll-*a* concentrations (Chl-*a*) between the simulated field and the data (see Sect. 4.3). We changed the grazing function with the introduction of the preference parameter for the zooplankton for different types of plankton (Dadou et al., 2001, 2004), as well as the associated maximum growth rates and half saturation constants for ingestion. With these modifications, the general spatial distribution of the different types of plankton from the coast to the open ocean in the BUS is better simulated as compared to data (Kreiner and Ayon, 2008; Silio-Calzada et al., 2008).

This first adjusted version of the model constitutes the reference run for the following analyses of the parameters. Then, the values of key parameters were adjusted performing sensitivity analyses (Table 3). The methodology for these analyses consists in arbitrarily changing the value of these key parameters for the reference run. Parameters are modified one by one and their reference values are increased or decreased by a factor of 2 up to a factor of 10. For each analysis, the annual means of the simulated fields were compared with the annual climatologies of nitrate and oxygen concentrations from the CSIRO Atlas of Regional Seas (CARS, 2006) and SeaWiFS Chl-*a* (see details on Sect. 3). The parameter value is chosen such as the difference between the simulated fields and the data for nitrates, oxygen and Chl-*a* is the smallest among the different tests we made. These adjustments are illustrated in Fig. 3 for the three parameters $K_{ND4}$, $w_{D_L}$ and $K_{NO_{3_{P_S}}}$ (Table 3) using different representative profiles.

The decrease by a factor of 10 of the DON mineralization parameter ($K_{ND4}$) induces a better agreement between the simulated fields and the data. It results in an improvement of 20% for the 0–100 m integrated nitrate concentrations along the east-west profile averaged between 22° S and 24° S (Fig. 3a) and of 10% for the gradient in the





BGD
8, 3537–3618, 2011



first 100 m of the vertical profile of oxygen concentrations (Fig. 3c). The doubling of the sedimentation sinking velocity parameter ($w_{D_L}$) leads to a decrease of 15% of the 0–100 m integrated nitrate concentrations, mainly outside the continental shelf (Fig. 3a), and a decrease of 10% of the oxygen concentrations below 200 m on the continental shelf, both in better agreement with data (Fig. 3c). The very small effect of doubling the phytoplankton nutrient half-saturation coefficient ($K_{NO_{3_{PS}}}$) on surface Chl-*a* (Fig. 3b), nitrate and oxygen concentrations justifies our choice to keep this parameter at a low value ($K_{NO_{3_{PS}}} = 0.5\,\mathrm{mmol\,N\,m^{-3}}$ as for the reference run). Using these sensitivity analyses, we also decreased the small zooplankton specific excretion rate $\gamma_{Z_S}$ by a factor of 2 in order to add an additional decreasing effect on the ammonium and nitrite concentrations, already existing with the $w_{D_L}$ and $K_{ND4}$ adjustments (data not shown). Finally, the maximum growth rate of the large phytoplankton (diatoms) had to be reduced from $0.8356\,\mathrm{d^{-1}}$ (Koné et al., 2005) to $0.6\,\mathrm{d^{-1}}$ (Fasham et al., 1990; Oschlies and Garcon, 1999; Huret et al., 2005) to obtain a better agreement between the simulated primary production and the BENEFIT data from Barlow et al. (2009) as well as the data from the Atlantic Meridional Transect (AMT) in May 1998 (AMT 6 cruise), especially in the coastal area (see Sect. 4.3).

### 2.3 The Namibian configuration

The ROMS Namibian configuration (Fig. 1) is built on a Mercator grid, spanning 5° E to 17° E and 19° S to 28.5° S with a horizontal resolution of 1/12° (ranging from 8.15 km in the south to 8.8 km in the north). The grid has 32 sigma-levels stretched so that near-surface resolution increases. In the coastal area, with a minimum depth of 75 m, the thickness of the first (at the bottom of the ocean) and last (near the ocean-atmosphere interface) levels is 11.4 m and 0.4 m, respectively. In the open-ocean area, with a maximum depth of 5000 m, the thickness of the first and last levels is 853.5 m and 5 m, respectively. Bottom topography from 1′ GEBCO (General Bathymetric Chart of the Oceans: http://www.gebco.net) (Fig. 1) product has been interpolated onto the model grid, smoothed as in Penven et al. (2005) in order to reduce pressure gradient errors.





BGD
8, 3537–3618, 2011



The ROMSTOOLS package (Penven et al., 2008, http://roms.mpl.ird.fr) has been used to build the model grid, atmospheric forcing, initial and boundary conditions.

The Namibian configuration used in this study is a small domain which is a sub-domain of the SAfE HR climatological configuration (Veitch et al., 2009) (Fig. 1). For temperature, salinity, free surface and the velocity (zonal and meridional components), the initial conditions come from 1 January of the 10th year of SAfE HR (Veitch et al., 2009); the open boundary conditions are also provided by the 10th year of this simulation for which variables have been averaged every 5 days.

A 1/2° resolution QuikSCAT (Liu et al., 1998) monthly climatological wind stress (courtesy of N. Grima, LPO, Brest, France) based on data spanning from 2000 to 2007 is used to force the model at the surface. Surface heat and salt fluxes are provided by 1/2° resolution COADS-derived monthly climatology (Da Silva et al., 1994). An air-sea feedback parameterization term, using the 9-km Pathfinder climatological Sea Surface Temperature (SST) (Casey and Cornillon, 1999), is added to the surface heat flux to avoid model SST drift (Barnier et al., 1995; Marchesiello et al., 2003). A similar correction scheme is used for Sea Surface Salinity (SSS) because of the paucity of evaporation-precipitation forcing fields as in Veitch et al. (2009).

For the biogeochemistry, the initial and the open boundary conditions for $NO_3$ and $O_2$ concentrations are provided by the month of January and the monthly climatology of the CARS database (2006), respectively. Other biogeochemical tracers are initialized using a constant profile (see Table 1); the same constant profiles are used for the open boundary conditions.

The simulation is run for a total of 12 yr. A physical spin-up is performed over 7 yr, as the model needs a few years to reach a stable annual cycle, then the coupled physical/biogeochemical model is run for 5 yr. The last year of simulation (year 12) will be analyzed in the following sections of the paper, except for the time evolution at 23° S where we consider the last three years of simulation after the spin-up of two years. The time step of the physical model is 15 min, and the biological time step is 5 min. Outputs are saved as 3-daily averages.





BGD
8, 3537–3618, 2011



## 3 Satellite and in-situ data used

In the studied area, simulated fields are compared with different types of available data sets.

Chl-*a* from the monthly climatology SeaWiFS products of level 3-binned data (9 km, version 4, O'Reilly et al., 2000), from 1997 to 2009, processed by the NASA Goddard Space Flight Center and distributed by the DAAC (Distributed Active Archive Center) (McClain et al., 1998), are used for comparison with surface simulated Chl-*a*. Simulated Chl-*a* is the sum of flagellate and diatom concentrations expressed in N units and converted into Chl-*a* (mg Chl $m^{-3}$) using a variable ratio described in Appendix A.

Different sections and stations are used for the model/data comparison. Their positions are shown in Fig. 4. Temperature, salinity, oxygen, nutrients, Chl-*a*, primary production, and mesozooplankton data were collected in May 1998 during the AMT 6 cruise (Aiken, 1998; Aiken and Bale, 2000; Aiken et al., 2000). Samples were collected during expeditions M57/2 of R/V *Meteor* February 2003 (Zabel et al., 2003; Kuypers et al., 2005) and AHAB1 of R/V *Alexander von Humboldt* in January 2004 (Lavik et al., 2009), and allowed to estimate temperature, salinity, oxygen and nutrients in the Namibian upwelling system. In October 2006, the Danish Galathea expedition crossed the BUS. Measurements of temperature, salinity, oxygen, nutrients, and Chl-*a* were collected (courtesy of L. L. Søerensen, National Environmental Research Institute, Denmark) at different stations and along a vertical section (triaxus system undulating vertically and laterally off the stern of the ship). A mooring located on the outer shelf at 23° S in Walvis Bay between 1994 and 2004 (Monteiro and van der Plas, 2006) allowed to obtain a time series of temperature, salinity and oxygen. Measurements of copepod abundance integrated over 200 m, from the coast (14.5° E) to 70 nautical miles (13.23° E) at 23° S in Walvis Bay, were collected between 2000 and 2007 (Kreiner and Ayon, 2008). Primary production estimations were effectuated during winter 1999 and summer 2002, as part of the BENEFIT program (Barlow et al., 2009). The CSIRO Atlas of Regional Seas allowed to establish monthly climatologies with 1/2° of resolution for





BGD
8, 3537–3618, 2011



temperature and salinity fields (CARS, 2009), and oxygen and nitrate concentrations (CARS, 2006). The World Ocean Atlas (WOA) 2001 includes a global climatology of Chl-*a* (Conkright et al., 2002). The AMT 17 cruise in November 2005 estimated DON concentrations in the Southern Benguela. For the first time in the Namibian upwelling system, $N_2O$ samples were collected at 9 stations off Walvis Bay at around 23° S during the FRS Africana cruise, in December 2009 within the framework of the GENUS project (Geochemistry and Ecology of the Namibian Upwelling System). The collected samples were poisoned with mercuric chloride on board and measurements were done after the cruise at IFM-GEOMAR, Germany by using the static equilibration method according to Walter et al. (2006).

All data enumerated above will be compared to simulated ones for the same geographical positions (except for DON because there are no available measurements in the Namibian upwelling system) and the same climatological months. Simulated oxygen concentrations are converted in ml $O_2$ $l^{-1}$ for comparison with in-situ data.

## 4 Model/data comparison

To compare simulated fields $m$ and data $d$ (in-situ and satellite data considered as the reference), different statistical metrics are selected: the mean ($M$), the bias ($M_m - M_d$), the Root Mean Square (RMS), the standard deviation ($\sigma$), and the correlation coefficient ($R$). The centered pattern RMS difference ($E'$) is formulated as $E'^2 = \sigma_m^2 + \sigma_d^2 - 2\sigma_m\sigma_d R$. The centered pattern RMS difference and the two standard deviations are normalized by the standard deviation of the data $\sigma_d$. Then, the normalized standard deviation of the simulated field is $\sigma^* = \sigma_m^* = \sigma_m/\sigma_d$, the normalized standard deviation of the data is $\sigma_d^* = 1$, and the normalized centered pattern RMS difference becomes $E'^* = E'/\sigma_d = \sqrt{\sigma^{*2} + 1 - 2\sigma^* R}$. The statistical information ($E'^*$, $\sigma^*$, $R$), referred as "pattern statistics", is summarized in Taylor's diagrams (Taylor, 2001).





BGD
8, 3537–3618, 2011



### 4.1 Temperature, salinity, and density

For the temperature field (Fig. 5a), the correlation coefficient between simulated fields and data is above 0.93 for all stations and sections except for the Galathea data (surface and station data; $R = 0.86$). The normalized standard deviation for temperature is between 0.9 and 1.2 for all comparisons; except for the Galathea data ($\sigma^*$ is between 1.3 and 1.4). The normalized centered pattern RMS difference is less than 0.4, except for the Galathea data ($E'^* = 0.5$ for triaxus data, or a RMS difference of 1.41 °C; $E'^* = 0.67$ for surface and station data, or a RMS difference of 1.43 °C). The differences between model and data averages (called bias) for temperature vary from 0.25 to 1.2 °C along the METEOR 57/2 sections, from −0.33 to 0.52 °C for the AHAB1 sections, from 0.6 to 1 °C for the Galathea data, and from 0.2 to 1.2 °C for the AMT 6 data.

For the salinity field (Fig. 5b), the correlation coefficient between simulated fields and data is above 0.74 for all stations and sections, except for Galathea data (station and surface data; $R = 0.62$). The normalized standard deviation is between 0.55 and 1.2 for all data, except for four Galathea triaxus ($\sigma^* = 1.55$). The normalized centered pattern RMS difference is less than 0.7, except for the Galathea surface and station data ($E'^* = 0.95$, or a RMS difference of 0.15). Biases for salinity vary from −0.05 to 0.08 along the METEOR 57/2 sections, from −0.2 to −0.001 for the AHAB1 sections, from 0.04 to 0.1 for Galathea data, and from −0.22 to −0.009 for the AMT 6 data.

The same comparison is made for the density field. Density is computed from temperature and salinity in-situ data, using the same Jackett and McDougall (1995) relationship that one used in ROMS. The correlation coefficient between simulated and in-situ density is above 0.9 for all stations and sections (Fig. 5c). The normalized standard deviation is between 0.85 and 1.4 for all comparisons; and the normalized centered pattern RMS difference is less than 0.52 (the range of RMS difference is between 0.13 and 0.29 $\mathrm{kg\,m^{-3}}$). Bias for density varies from −0.26 to −0.06 $\mathrm{kg\,m^{-3}}$.

In general, the model outputs overestimate the temperature field, and underestimate salinity and density fields as compared to in-situ data. These biases are mainly





BGD
8, 3537–3618, 2011



observed in the surface layer (0–100 m) over the continental shelf. No clear latitudinal trend can be highlighted. The results of these statistics point out an important interannual variability for the in-situ data which is not represented by our simulation. Indeed, the monthly climatological fields (winds, heat and fresh water fluxes) used to force the model are repeated each year, with a linear interpolation between each month, so the forcing fields are smoothed in time.

To complete the model/data comparison, the same statistics for the annual mean and the seasonal cycle are computed between the simulated fields and the climatology from CARS database (2009). The comparison between seasonal fields is performed between the surface and 600-m depth. Below this depth, statistics do not show seasonal variation (not shown). The annual fields are also compared in the top 600 m as well as over the whole water column. The statistics were added in the Taylor's diagrams for temperature, salinity, and density (see the last six points in Fig. 5a, b, and c). The correlation coefficient between simulated fields and CARS database (2009) is above 0.98 for temperature, and above 0.96 for salinity and density. The normalized standard deviation is between 0.9 and 1 for temperature, between 0.8 and 1 for salinity, and between 0.85 and 1 for density. The normalized centered pattern RMS difference is less than 0.21 (or a RMS difference of 0.9 °C) for temperature, 0.3 (or a RMS difference of 0.1) for salinity, and 0.3 (or a RMS difference of 0.17 $kg\,m^{-3}$) for density. Biases vary between 0.09 and 0.29 °C, −0.05 and −0.01 for salinity, −0.07 and −0.02 $kg\,m^{-3}$.

To illustrate the above Taylor's diagrams, two types of model/data distributions in space and time are presented along a section (23° S; Figs. 6 and 7) and at a mooring point (23° S–14° E; Fig. 11). Monthly averaged simulated fields and in-situ measurements of temperature, salinity and density along the 23° S METEOR 57/2 section (east-west direction in February 2003) are displayed in Fig. 6. On the shelf, temperature and salinity isocontours rise to the surface, which is the signature of the coastal upwelling off Namibia. Vertical temperature gradient is well simulated over the 23° S section. In the top 100 m, simulated salinity is weaker than the observed one. The detailed analysis of all sections and stations in the studied area shows similar results





BGD
8, 3537–3618, 2011



as for the 23° S METEOR 57/2 section. Figure 7 presents the annual mean of temperature, salinity, and density at 23° S as compared with the annual climatology from CARS database (2009). Simulated fields are in agreement with the data: the vertical profile of temperature, salinity, and density are correctly simulated, although simulated salinity is weaker than measured salinity in the surface one, especially near the coast. This bias seems to come from the SSS corrections used in the model configuration. Indeed, the SSS values from the COADS climatology used for the correction scheme in the salt fluxes (Sect. 2.3) are lower than in-situ data and CARS climatology (2009) at 23° S (not shown).

The temporal evolution of the vertical profiles of simulated temperature and salinity at 23° S–14° E (Fig. 11) is compared to the time series at this Walvis Bay mooring (Fig. 4 for location) (see figure 5-3 from Monteiro and van der Plas, 2006). The same vertical structure in time is observed between the simulated fields and in-situ data. Temperature around 17–18 °C is observed each summer in the surface layer, isotherms 13 °C and 10 °C are situated around 100 and 300-m depth, respectively. Isohaline 35 is located at a mean depth of 200 m, with salinity up to 35.2 between the surface and 100-m depth, and fresher water intrusions around 34.8 occur each year at 300-m depth.

These statistics show that the model is able to simulate the annual mean and seasonal cycle for temperature, salinity, and density over the Namibian upwelling system despite a lower standard deviation.

### 4.2 Oxygen, nitrate, nitrite, and ammonium

The model correctly simulates the OMZ located along the continental slope (Figs. 8a and 9a), with more depleted waters in the northern part of the domain (between 19° S and 24–25° S) where the South Atlantic Central Waters (SACW; Mohrholz et al., 2008) are present. The differences between model and data averages for oxygen concentrations are always positive from 0.14 to 0.66 ml $O_2$ $l^{-1}$ along the METEOR 57/2 sections, from 0.03 to 1.6 ml $O_2$ $l^{-1}$ for the AHAB1 sections, from 0.18 to 0.8 ml $O_2$ $l^{-1}$ for the Galathea data, and 0.68 ml $O_2$ $l^{-1}$ for the AMT 6 data. This slight bias is mainly due





BGD
8, 3537–3618, 2011



to the overestimation of oxygen concentrations on the continental shelf for water-depth above 200 m. The correlation coefficient between simulated and in-situ oxygen concentrations varies between 0.55 and 0.97 for all data (Fig. 10a). The normalized standard deviation is lower than 1 for all comparisons. Standard deviation or variations of the simulated oxygen concentrations are lower than for in-situ measurements, mainly associated with interannual variability in the BUS. The normalized centered pattern RMS difference is less than 0.85 for all data. The RMS difference is between 0.34 and 2.35 ml $O_2$ $l^{-1}$.

To complete the statistics, the seasonal cycle and annual mean of simulated oxygen concentrations are compared with CARS database (2006). For all comparisons with CARS, the correlation coefficient is between 0.87 and 0.93, and the normalized standard deviation is between 0.85 and 0.95 (Fig. 10a). Biases vary between −0.1 and 0.09 ml $O_2$ $l^{-1}$. Compared to the CARS database (2006) (Fig. 9a), the vertical structure of oxygen concentrations is well simulated, except on the continental shelf where the OMZ occurs. In our simulation, the OMZ is located on the slope as for the CARS database (2006) but does not extend enough on the continental shelf. The same observation can be made when the temporal evolution of the vertical profiles of oxygen concentrations at 23° S–14° E (Fig. 11) is compared with the time series of oxygen concentrations at the Walvis Bay mooring (see figure 5-3 from Monteiro and van der Plas, 2006). The oxygen seasonal cycle is correctly represented. Concentrations between 6 and 7 ml $O_2$ $l^{-1}$ are well simulated close to the surface, while they are frequently lower than 1 ml $O_2$ $l^{-1}$ at depth. However, concentrations below 0.5 ml $O_2$ $l^{-1}$ are frequently recorded at this mooring while they remain higher than 0.5 ml $O_2$ $l^{-1}$ in our simulation. So, the model correctly simulates the vertical distribution of oxygen but in-situ concentrations are more depleted at depth than the simulated ones. We will comment this difference in the following paragraph.

At the surface of the domain, simulated and in-situ nitrate concentrations are less than 1 mmol N $m^{-3}$ in the open ocean (Figs. 8b and 9b) and higher than 16 mmol N $m^{-3}$ along the coast. The pool of high nitrate concentrations (around 30–35 mmol N $m^{-3}$)





BGD
8, 3537–3618, 2011



is located at depth between 200 and 1500 m (with variations depending on latitude and related to the upwelling cells along the coast). The differences between model and data averages for nitrate concentrations are from −2.7 to −1.66 mmol N $m^{-3}$ along the METEOR 57/2 sections, from −5 to 1.66 mmol N $m^{-3}$ for the AHAB1 sections, −0.02 mmol N $m^{-3}$ for the Galathea stations, and −7.9 mmol N $m^{-3}$ for the AMT 6 data. Hence, simulated nitrate concentrations are in general underestimated. The correlation coefficient between simulated and in-situ nitrate concentrations is between 0.8 and 0.94 for Galathea, AMT 6, and METEOR 57/2 data, with normalized standard deviations between 0.59 and 1.21, and normalized centered RMS differences less than 0.65 (RMS difference: 6.1 mmol N $m^{-3}$) (Fig. 10b). The statistics are worse for AHAB1 data in January 2004, but this period was particular because an important sulphidic event was recorded in the continental shelf waters off Namibia (Lavik et al., 2009) during this cruise. North of 27° S, oxygen-depleted waters ($O_2 < 0.1$ ml $O_2$ $l^{-1}$) were recorded below 60-m depth. In oxygen-depleted environments, the best electron acceptor for anoxic remineralization (denitrification) is nitrate. When oxygen and nitrate are depleted, sulfate reduction produces toxic hydrogen sulfide, as measured during the AHAB1 cruise. This extreme event generally occurs on or close to the sediments on the continental shelf, and our biogeochemical model does not include the sediment processes. In order to improve our model and simulate very low oxygen concentrations on the continental shelf, a sediment module has to be added to BioBUS.

As for the other variables, the seasonal cycle and annual mean of simulated nitrate concentrations are now compared with CARS database (2006). The correlation coefficient is higher than 0.94, and the normalized standard deviation is between 0.9 and 1.05. The normalized centered pattern RMS difference is less than 0.35 (or a RMS difference of 3.4 mmol N $m^{-3}$) for all comparisons with CARS climatology (2006) (Fig. 10b). Biases vary between −2.03 mmol N $m^{-3}$ in winter and 0.6 mmol N $m^{-3}$ in summer. The comparison between simulated fields and the CARS database (2006) (Figs. 9b and 10b) confirms that our model correctly simulates the seasonal cycle and annual mean of nitrate concentrations.





BGD
8, 3537–3618, 2011



The other nutrients, i.e. nitrite and ammonium, present very low values in the simulation with maximum value of 0.14 and 0.4 mmol N $m^{-3}$, respectively, located in the surface layer above the continental shelf. These two nutrients are fastly transformed in nitrate by the nitrification processes. For the AHAB1 cruise, concentrations up to 1 and 4 mmol N $m^{-3}$ were measured for nitrite and ammonium concentrations, respectively. These high values were principally observed on the continental shelf. The Galathea cruise measured nitrite concentrations up to 0.67 mmol N $m^{-3}$ in the studied area. During this cruise, ammonium concentrations below the detection level of 0.3 mmol N $m^{-3}$ were found all over the region, and the model is able to reproduce this pattern. During AMT 6 cruise, nitrite was measured at four stations in our studied area. Concentrations vary from 0.01 to 0.43 mmol N $m^{-3}$. Only two measurements of ammonium concentrations are available for this latter cruise: 0.62 mmol N $m^{-3}$ at 161-m depth and 3.13 mmol N $m^{-3}$ at 22-m depth (located at the same station 26.7° S–14.25° E). We do not have enough in-situ measurements of nitrite and ammonium concentrations to conclude, but simulated fields seem to have the same order of magnitude as in-situ data, maybe at the lower limit of the measured concentrations.

The model is able to simulate the annual mean and seasonal cycle for nitrate, and oxygen concentrations. Vertical gradients of simulated oxygen and nitrate concentrations as well as horizontal distributions give satisfying results, except oxygen concentrations near the sediment-water interface over the continental shelf. Simulated nitrite and ammonium concentrations are within the range of available in-situ data.

### 4.3 Chlorophyll-*a* and total primary production

Simulated surface Chl-*a* are around 0.25 mg Chl $m^{-3}$ offshore, being higher than those derived from SeaWiFS sensor (0.2 mg Chl $m^{-3}$; Fig. 12). Chl-*a* increase up to 10 mg Chl $m^{-3}$ at the coast (Fig. 12) in the model, in agreement with satellite data. High coastal simulated Chl-*a* exhibit a larger extension in the southern part of the studied domain, while they stay close to the coast in the northern part. On both data sets (satellite and simulated data), the onshore-offshore gradient is stronger in the southern





BGD
8, 3537–3618, 2011



part of the domain, while it is more diffusive in the northern part. The simulated Chl-*a* is now compared with the annual WOA climatology (2001; Conkright et al., 2002) along three vertical sections (21.5° S, 23.5° S, and 25.5° S; Fig. 13) in order to evaluate the performance of the modeling experiment in reproducing the vertical distribution. At 100-m depth, simulated and in-situ Chl-*a* are lower than 0.2 mg Chl $m^{-3}$. Maximum Chl-*a* are observed between the surface and 40–50 m depth in both data sets. At 21.5° S and 23.5° S, simulated Chl-*a* are lower than in-situ data in the surface layer; high simulated Chl-*a* are confined close to the coast. As the resolution of the WOA climatology (2001; Conkright et al., 2002) is too coarse, we used in-situ data from the Galathea and AMT 6 cruises to evaluate the simulated distribution of Chl-*a*.

Concerning the Galathea cruise (October 2006), three values of Chl-*a* in Walvis Bay (St. 6.7, in the middle of the domain) are available: one estimation at 10-m depth (1.16 mg Chl $m^{-3}$), another at 75-m depth (0.14 mg Chl $m^{-3}$), and a value integrated over the first 71-m depth (57.8 mg Chl $m^{-2}$). At the same location and same depths, simulated Chl-*a* are equal to 1.5 mg Chl $m^{-3}$, 0.2 mg Chl $m^{-3}$, and 69.5 mg Chl $m^{-2}$, respectively, so in close agreement with measurements. During the AMT 6 cruise in May 1998, vertical profiles of Chl-*a* were estimated by four different sources (E. Fernandez, P. Holligan, R. Barlow, and the British Oceanographic Data Center; Barlow et al., 2002, 2004) at three stations situated in the middle of our domain (St. 14, 15, and 16; Fig. 14). Vertical profiles of simulated Chl-*a* are within the different estimations. The sub-surface maximum (between 10 and 40 m) observed at St. 15 is well represented by the model with Chl-*a* reaching 1.4 mg Chl $m^{-3}$. At 62-m depth (St. 15), observed Chl-*a* are between 0.43 and 0.81 mg Chl $m^{-3}$, and simulated concentration is equal to 0.4 mg Chl $m^{-3}$. The vertical structures as well as the range of the simulated Chl-*a* are quite in agreement with the few available data.

On average over the year and the domain, the nanophytoplankton contribution to total simulated Chl-*a* represents 45% but exhibits an important spatial variability. In the open ocean, the contribution of nanophytoplankton is significant (50–70% of total Chl-*a*), while the microphytoplankton clearly dominates (80–100% of total Chl-*a*) along the





BGD
8, 3537–3618, 2011



coast. Based on satellite observations, Silio-Calzada et al. (2008) estimated that 39% of the total Chl-*a* are represented by nanophytoplankton on annual mean and over the same domain. This plankton community contributes to 50% in the open ocean and less than 20% along the coast. The model is in agreement with those satellite estimations. Silio-Calzada et al. (2008) also assessed that 24% of the total Chl-*a* are due to picophytoplankton in the Namibian ecosystem, with an increasing contribution as we move off the coast. In the eastern part of the domain, picophytoplankton contributes to 40% of total Chl-*a*. This phytoplankton population is not taken into account in BioBUS, so its contribution is partitioned between diatoms and flagellates. However, results from Silio-Calzada et al. (2008) should be taken with caution since their algorithm has not been validated with in-situ data in the BUS.

Simulated total primary production is now compared with the BENEFIT data from Barlow et al. (2009). During summer (February–March), simulated total primary production integrated over the euphotic zone reaches $6\,g\,C\,m^{-2}\,d^{-1}$ near the coast. In winter (June–July), it reaches $3\,g\,C\,m^{-2}\,d^{-1}$ near the coast. In our modeling experiment, the Namibian system appears to be twice more productive in summer than in winter. Along the Namibian coast, Barlow et al. (2009) estimated total primary production between 0.39 and $8.83\,g\,C\,m^{-2}\,d^{-1}$ during February–March 2002, and between 0.14 and $2.26\,g\,C\,m^{-2}\,d^{-1}$ during June–July 1999. Spatial variations are important. For example, between St. FM18, FM19 and FM20 (located close to the coast; see Fig. 1 in Barlow et al., 2009), primary production varies from 1.5 to $6.7\,g\,C\,m^{-2}\,d^{-1}$ during summer 2002. At St. FM 24 located more offshore, primary production was measured at $2\,g\,C\,m^{-2}\,d^{-1}$, the model giving the same value for this location. Simulated total primary productions are within the range of values estimated by Barlow et al. (2009) for summer time, but are much higher than those measured during winter 1999. But one should notice that 1999 was a particular year since a Benguela Niño event occurred in April (Mohrholz et al., 2004). The Benguela Niño event is characterized by an abnormal southern position of the Angola-Benguela frontal zone, leading to a surface warming of the south-west African coastal waters. These positive SST anomalies can





BGD
8, 3537–3618, 2011



remain some months (Shannon et al., 1986). Therefore the upwelling of nutrient-rich waters decreases and primary production is lower than usual for some time. Siegfried et al. (1990) reported that during previous Benguela Niño events, primary productivity has been reduced by more than two thirds.

During the AMT 6 cruise in May 1998 (Aiken, 1998; Aiken and Bale, 2000; Aiken et al., 2000), total primary production was estimated at three stations within our studied area. Simulated and in-situ total primary productions were integrated over the euphotic zone as Barlow et al. (2009) (simulated euphotic zone is between 20 and 37-m depth at the three studied stations). At St. 12, the simulated primary production is higher ($3.9\,g\,C\,m^{-2}\,d^{-1}$) than in-situ primary production ($1.6\,g\,C\,m^{-2}\,d^{-1}$). At St. 15 (St. 18), simulated and in-situ values are similar, with 3.3 ($3.55\,g\,C\,m^{-2}\,d^{-1}$) and $3.26\,g\,C\,m^{-2}\,d^{-1}$ ($3.32\,g\,C\,m^{-2}\,d^{-1}$), respectively. At the three stations, the surface primary production is higher than in-situ data, the difference decreases until ~25-m depth. Below this limit, simulated and in-situ estimations of primary production are similar, and they are close to 0 at 50-m depth.

Spatio-temporal variability of primary production is pretty well captured in our modeling experiment even if direct comparisons are difficult to analyze in such a dynamic environment.

### 4.4 Zooplankton and DON

The temporal evolution of simulated copepod (mesozooplankton: large zooplankton or $Z_L$ in the model) abundance (number of individuals per $m^2$: $no\,m^{-2}$) at 23° S is compared with in-situ data from Kreiner and Ayon (2008) (Fig. 15). Integrated over 200-m depth, in-situ data between 2000 and 2007 present an important interannual variability. However, the maximum abundance is usually observed during the first part of the year (summer–early fall, with $1.10^5$ to $7.10^5$ $no\,m^{-2}$) and is located between 10 (14.2° E) and 50 nautical miles (13.5° E) off the coast (Kreiner and Ayon, 2008). To compare with the same units as Kreiner and Ayon (2008), we used a mean dry weight of individual animal of 40.75 µg for each individual. It corresponds to a mean dry





BGD
8, 3537–3618, 2011



mass for Calanoides Carinatus (juvenile, and adult stages) as estimated by Huggett et al. (2009), a major copepod species in the Namibian system. Biomass was converted in terms of carbon by assuming that 40% of the dry weight was carbon (Peterson et al., 1990). The C/N ratio of 5.36 used for mesozooplankton biomass comes from AMT 6 (Aiken, 1998; Aiken and Bale, 2000; Aiken et al., 2000) estimations in this area. As shown in Fig. 15, the model simulates a maximum of copepod abundance during summer–early fall, situated at the same distance from the coast as in-situ data. Each year of the climatological simulation, the simulated copepod abundance varies between $1.10^5$ and $5.10^5$ no $m^{-2}$.

During AMT 6 cruise, zooplankton was estimated at three stations (St. 15, 12, and 7; see Fig. 4). Data from different size classes (200–500 µm, 500–1000 µm, 1000–2000 µm, >2000 µm) were integrated over 200-m depth except for St. 12 where integration were performed over 100-m depth. To compare with our simulation, we only take into account the fraction comprised between 200 and 2000 µm, usually considered as mesozooplankton (copepods in the model). During the cruise, mesozooplankton was estimated at a value of 796.5 mg N $m^{-2}$ at St. 15, 2204.6 mg N $m^{-2}$ at St. 12, and 357.5 mg N $m^{-2}$ at St. 7. For the same climatological month and the same locations, the simulated concentrations are around 750, 200, and 150 mg N $m^{-2}$. At St. 15, simulated and in-situ concentrations have similar values. At St. 12 and 7, simulated concentrations are much lower than in-situ data maybe due to in-situ sampling collected in an enriched structure (filament, eddy). Indeed, if we do not take the value at exactly the same location, but in a physical structure, simulated mesozooplankton concentrations can reach 1100 mg N $m^{-2}$. This range of value comes closer to the in-situ observations.

Simulated semi-labile DON is compared with data from the AMT 17 cruise conducted in November 2005 (Holligan, 2005). This cruise did not cross the Namibian upwelling system but crossed the offshore region of the Southern Benguela upwelling system. No other estimation of DON is available at our knowledge. To estimate the semi-labile part of in-situ DON measurements, we assumed the deepest value for each station as





BGD
8, 3537–3618, 2011



refractory DON, and we removed this refractory part (assumed constant with depth) of the vertical profile of DON. Simulated vertical profiles of semi-labile DON concentrations were taken offshore, one in a physical structure (a filament) and another one outside of this structure (Fig. 16). Simulated and in-situ profiles are not directly comparable but in-situ concentrations give an indication on the profiles we can expect to find offshore of our domain. Simulated DON concentrations are within the range of in-situ concentrations (Fig. 16). The three eastern stations of AMT 17 seem to be out off a physical structure, while the station at 33.9° S–10.3° E could be in a filament or an eddy.

### 4.5 $N_2O$ distribution

In Fig. 17, the vertical sections of temperature, salinity, and oxygen concentrations off Walvis Bay derived from modeled fields show the signature of an upwelling event due to intense alongshore winds. A similar situation was observed during the FRS Africana cruise in December 2009 as strong winds lead to upwelling of oxygen-depleted subsurface waters intersecting the surface within a narrow strip (15–20 nm) along the coast around Walvis Bay (Mohrholz et al., 2009 in Cruise Report from Ekau and Verheye, 2009).

In-situ $N_2O$ concentrations reached up to approximately 40 nmol $N_2O$ $l^{-1}$ in oxygen-depleted waters in the water column onto the shelf, and at the shelf break near the water-sediment interface and tend to decrease with increasing $O_2$ concentrations (Fig. 17c and d). Simulated $N_2O$ concentrations have similar values as compared to data for waters with $O_2$ concentrations above 2.6 ml $O_2$ $l^{-1}$ (Fig. 17c and d). For lower $O_2$ concentrations, simulated $N_2O$ concentrations are underestimated as compared to measured ones, with a maximum of 20 nmol $N_2O$ $l^{-1}$ over the shelf and shelf-break (Fig. 17d). The parameterization used in BioBUS (see Appendix A) from Nevison et al. (2003) only takes into account $N_2O$ formation associated with oxygen consumption during nitrification process. A more complex parameterization from Freing et al. (2009)





BGD
8, 3537–3618, 2011



will probably improve results for the $N_2O$ distribution in the whole ocean including OMZ. This parameterization will be implemented and tested in BioBUS in a future work.

## 5 Nitrogen budget in the Walvis Bay area: nitrogen transfers and air-sea $N_2O$ fluxes

The nitrogen (N) budget is performed around Walvis Bay between 22° S and 24° S and from the coast to 12.5° E. Walvis Bay is chosen because the OMZ is well developed in this area (Mohrholz et al., 2008; Monteiro et al., 2008). To understand the horizontal and vertical transfers of N from the coast to the open ocean, the studied area is divided in two sub-domains: the coastal domain which represents the continental shelf from the coast to the 200-m isobath and the continental slope domain which is considered to be situated between the 200-m isobath and the 2500-m isobath. These two sub-domains are divided in three layers: the surface layer down to 100-m depth (maximum depth of the mixed layer in the ocean in austral winter); the intermediate layer between 100 and 600-m depth where the OMZ is located; and the oxic bottom layer between 600 and 5000-m depth. Note that the volume of each sub-domain is different, and then integrated fluxes (in $10^{10}$ mol N yr$^{-1}$) presented in Figs. 18 and 19 cannot be directly compared from a sub-domain to the other. In the following, the area called "entire Walvis Bay domain" corresponds to 22° S–24° S, from the coast to 10° E. For comparisons with other studies, we took a C/N Redfield ratio (106/16; Redfield et al., 1963) for the conversion of fluxes from nitrogen to carbon.

### 5.1 Physical forcing and associated export

As shown in Fig. 18, two main areas of upwelling are found. Nitrate-rich SACW waters upwell over the slope ($17.7 \times 10^{10}$ mol N yr$^{-1}$) at 100-m depth: $8 \times 10^{10}$ mol N yr$^{-1}$ are upwelled at 50-m depth, $5.9 \times 10^{10}$ mol N yr$^{-1}$ advected onshore between 50 and 100 m and, and $8.6 \times 10^{10}$ mol N yr$^{-1}$ advected offshore between 50 and 100-m depth. Above





BGD
8, 3537–3618, 2011



the continental shelf off Walvis Bay area, $6.5 \times 10^{10}$ mol N yr$^{-1}$ upwell at 50-m depth. Then, the Ekman transport advects nitrate enriched waters offshore between 0 and 50-m depth: $9.2 \times 10^{10}$ mol N yr$^{-1}$ are advected between the continental shelf and the slope sub-domains, $16.8 \times 10^{10}$ mol N yr$^{-1}$ between the slope sub-domain and the open ocean. The alongshore Benguela current also advects nutrient-rich waters from the Lüderitz upwelling cell to the Northern Benguela system. As expected, the meridional advection due to the coastal Benguela current between 0 and 100-m depth has the most important contribution on the continental shelf ($9.6+2.7 = +12.3 \times 10^{10}$ mol N yr$^{-1}$) and decreases with distance to the coast ($5.3 + 3.5 = +8.8 \times 10^{10}$ mol N yr$^{-1}$ on the slope). In the coastal domain, the meridional advection of the Benguela current represents the main contribution for sustaining primary production (between 0 and 100-m depth). From the surface to 100-m depth, zonal advection exports nitrates ($9.2–5.9 = 3.3 \times 10^{10}$ mol N yr$^{-1}$) offshore from the coast to the slope sub-domain, 25.4 ($=16.8 + 8.6$) $10^{10}$ mol N yr$^{-1}$ from the slope sub-domain to the open ocean (Fig. 18).

Between 100 and 600-m depth, inshore zonal current advects nitrate enriched waters with an inshore decreasing contribution. At this depth range over the slope, the poleward undercurrent below the Benguela current advects nitrate enriched waters southward and represents a sink for the studied area with a maximum value over the continental slope.

## 5.2 Primary and secondary productions

Diatom biomass contributes to 99.2% of total primary production along the continental shelf, and 92% along the continental slope. Total primary production is largely sustained by nitrates: nitrates contribute to 87.7% of total primary production along the continental shelf and 80.8% along the slope. Primary production due to ammonium is not negligible and explains 11.9% of total primary production on the shelf and 17.9% on the slope. By contrast, primary production based on nitrite is weak; it only contributes to 0.4% of total primary production on the coast and 1.3% on the slope, due to a fast nitrification process and a very active upwelling.





BGD
8, 3537–3618, 2011



In our study, total primary production estimated around Walvis Bay is equal to $15.5 \times 10^2$ g C m$^{-2}$ yr$^{-1}$ over the continental shelf and $11.1 \times 10^2$ g C m$^{-2}$ yr$^{-1}$ over the slope domain. In the BUS, annual primary production has been estimated at $7.6 \times 10^2$ g C m$^{-2}$ yr$^{-1}$ by Ware (1992), $9.5 \times 10^2$ g C m$^{-2}$ yr$^{-1}$ by Carr (2002), $5.1 \pm 0.6 \times 10^2$ g C m$^{-2}$ yr$^{-1}$ based on the AMT data by Tilstone et al. (2009), and from $3.7 \times 10^2$ up to $9.5 \times 10^2$ g C m$^{-2}$ yr$^{-1}$ using satellite primary production models (Tilstone et al., 2009). Brown et al. (1991) estimated the primary production in the Northern Benguela system at $4.3 \times 10^2$ g C m$^{-2}$ yr$^{-1}$ inshore the 500-m isobath. Our estimation over the entire Walvis Bay domain is $10 \times 10^2$ g C m$^{-2}$ yr$^{-1}$, so higher than the estimation made by Brown et al. (1991) for the Northern Benguela system, and closer to the estimation made by Carr (2002) and Tilstone et al. (2009) using primary production models based on satellite observations. This observation is not surprising as the primary production in the Northern Benguela system for latitudes between 20° S and 18° S are lower than the primary production around Walvis Bay which represents a very productive area as compared to other regions of the BUS.

Secondary production (or total grazing) includes grazing of phytoplankton (flagellates and diatoms) by zooplankton (ciliates and copepods) and grazing of ciliates by copepods. Over the continental shelf, 42% of total grazing is due to copepods, 87% of it being upon diatoms. Over the slope, copepods explain 60.2% of total grazing, and 79.6% is effectuated upon diatoms. Over the entire Walvis Bay domain, net assimilated grazing flux is estimated at $2.8 \times 10^2$ g C m$^{-2}$ yr$^{-1}$. Monteiro (2010) estimated the food web consumption term at $10^2$ g C m$^{-2}$ yr$^{-1}$ in the Northern Benguela system. Simulated zooplankton consumption is higher (×2.8) than those estimated by Monteiro (2010). As for primary production, the analysis in our study is performed on a very productive area (around Walvis Bay) which is smaller than the one considered in Monteiro (2010).





BGD
8, 3537–3618, 2011



### 5.3 Vertical export of POM and fixed inorganic N losses by denitrification and anammox

In the surface layer (0–100 m), the high biological activity produces a large amount of detritus and DON. This OM ($D_S$, $D_L$ and DON) is actively remineralized in the surface layer: 12.7 ($=5.9+6.8$) $\times 10^{10}$ mol N yr$^{-1}$ over the coast and 24.1 ($=8.8+15.3$) $\times 10^{10}$ mol N yr$^{-1}$ at the slope (Fig. 19). In the surface layer (0–100 m), an important vertical export production of PON is simulated. Large detritus is by far the main contributor to total vertical PON export: it contributes to 97.1% (or $5.1 \times 10^{10}$ mol N yr$^{-1}$) over the coast and 98.6% (or $9.2 \times 10^{10}$ mol N yr$^{-1}$) at the slope (Fig. 19). The annual mean simulated vertical PON export is equal to 2.5 mol N m$^{-2}$ yr$^{-1}$ (or $2 \times 10^2$ g C m$^{-2}$ yr$^{-1}$) on the continental shelf, slightly higher than Monteiro (2010) who estimated a sinking flux of particulate organic carbon (POC) to $2 \times 10^{13}$ g C yr$^{-1}$ (or $1.1 \times 10^2$ g C m$^{-2}$ yr$^{-1}$) in the Northern Benguela system. But, the same comment as for primary production and grazing can be made here: Walvis Bay is a very productive area and is not representative of the whole Northern Benguela system.

Simulated nitrification fluxes seem in agreement with in-situ estimations. Indeed, Molina and Farías (2009) measured the aerobic $NH_4^+$ oxidation rates (1st stage of nitrification) along the vertical profile of oxygen off Northern Chile. In the upper part of the oxycline (between 15 and 30-m depth), within the euphotic layer, aerobic $NH_4^+$ oxidation rates were detected between 0.16 and 0.79 µM d$^{-1}$ (or between 5.8 and 28.8 $\times 10^{-2}$ mol N m$^{-3}$ yr$^{-1}$). In our modeling experiment, the two nitrification stages have a maximum between 20 and 80-m depth, with values up to 8.9 and $8.6 \times 10^{-2}$ mol N m$^{-3}$ yr$^{-1}$ for the 1st and 2nd stages of nitrification, respectively. This estimate is between the values found by Molina and Farías (2009).

In the intermediate layer (between 100 and 600-m depth), processes of remineralization (oxic and anoxic) of the OM (here: $D_L$ and DOM; remineralization processes are between one and three order of magnitude lower





BGD
8, 3537–3618, 2011



for $D_S$ than for $D_L$ and DON in this intermediate layer) stay very active, with 0.9 ($=0.32+0.0013+0.57+0.008)\times10^{10}$ mol N yr$^{-1}$ over the coast and 5.6 ($=2.1+0.004+3.5+0.026)\times10^{10}$ mol N yr$^{-1}$ at the slope (Fig. 19). During remineralization processes, oxygen is consumed and low oxygen concentrations are frequently found between 100 and 600 m (intermediate layer) over the continental shelf and slope. OM remineralization due to denitrification process represents 0.03 ($=0.026+0.004)\times10^{10}$ mol N yr$^{-1}$ at the slope and 0.0093 ($=0.008+0.0013)\times10^{10}$ mol N yr$^{-1}$ on the coast (Fig. 19). This anaerobic remineralization associated to the anammox process contributes to a fixed inorganic N loss for the system: $4.8\times10^{7}$ mol N yr$^{-1}$ is lost on the shelf and $1.7\times10^{8}$ mol N yr$^{-1}$ on the slope (Fig. 19). In the bottom layer (between 600 m and 5000-m depth), the remaining detritus are remineralized under oxic conditions. Kuypers et al. (2005) and Lavik et al. (2009) found in situ values between 0.075 and 0.25 mmol $N_2$ m$^{-3}$ d$^{-1}$, mainly near the water-sediment interface in Walvis Bay (water depth lower than 200 m) for fixed inorganic N loss associated with denitrification. We underestimated this fixed inorganic N loss with a maximum simulated value of 0.035 mmol $N_2$ m$^{-3}$ d$^{-1}$ between 22° S and 24° S. As sediment processes are not taken into account in BioBUS, this underestimation is certainly associated with missing sediment processes. Indeed, a large fraction (1/2 to 3/4) of denitrification occur in the sediment and the other fraction in the water column (Devol, 2008). The same remark can be made for anammox process: in situ estimations varies between 0.01 and 0.2 mmol $N_2$ m$^{-3}$ d$^{-1}$ (Kuypers et al., 2005; Lavik et al., 2009) while the maximum simulated value is $1.7\times10^{-4}$ mmol $N_2$ m$^{-3}$ d$^{-1}$. In this modeling experiment, the anammox process is clearly underestimated as compared with in-situ estimations. It only generates a fixed inorganic N loss of $2\times10^{5}$ mol N yr$^{-1}$ on the shelf and $5.6\times10^{5}$ mol N yr$^{-1}$ on the slope. The explanation could come from the used formulation from Yakushev et al. (2007) for the anammox process which requires the simultaneous presence of $NO_2^-$ and $NH_4^+$. Indeed, $NO_2^-$ concentrations are generally very low in the marine environment as compared to $NO_3^-$, as in our studied area. Recent studies argue that microbial processes could be more complex than the





BGD
8, 3537–3618, 2011



ones parameterized in biogeochemical models. A coupling between aerobic (nitrification) and anaerobic (anammox) $NH_4^+$ oxidation (Woebken et al., 2007), as shown for the Black Sea (Lam et al., 2007), could be at work, producing $NO_2^-$ simultaneously with the consumption of this later during the anammox process. It could be of interest to take into account this coupling to correctly estimate the anammox process.

Inshore of the 600-m isobath, an important quantity of PON (principally large detritus) reaches the sediment before being remineralized. As explained in the previous section, the model does not include a sediment module; PON just accumulates on the floor artificially in the model, without further interaction with the overlying waters. The burial flux of PON in the sediment reaches 4.1 ($=3.3+0.8$) $\times 10^{10}$ mol N yr$^{-1}$ (or $1.6 \times 10^2$ g C m$^{-2}$ yr$^{-1}$) on the continental shelf (97.8% due to large detritus) and 1.25 ($=1.2+0.05$) $\times 10^{10}$ mol N yr$^{-1}$ (or $0.3 \times 10^2$ g C m$^{-2}$ yr$^{-1}$) at the slope (99.9% due to large detritus) (Fig. 19). Monteiro (2010) estimated the annual depositional loads of POC in the Northern Benguela system sediments to be $0.7 \times 10^{13}$ g C yr$^{-1}$, corresponding to a mean depositional flux rate of $0.4 \times 10^2$ g C m$^{-2}$ yr$^{-1}$ in the organic-rich surface sediments over the continental shelf.

### 5.4 Nitrogen transfers and nitrogen source for the South Atlantic Subtropical Gyre

Nitrogen input into the surface layer by vertical and meridional advection is compensated by offshore and downward exports (by advection and PON vertical sedimentation) of OM. In the surface layer (0–100 m) of the coastal and slope sub-domains, total export of organic N represents $21.5 \times 10^{10}$ mol N yr$^{-1}$ (which corresponds to $38.5 \times 10^{-3}$ mol N m$^{-3}$ yr$^{-1}$). Vertical sinking of POM represents 67.4% of this export ($14.5 \times 10^{10}$ mol N yr$^{-1}$ or $25.9 \times 10^{-3}$ mol N m$^{-3}$ yr$^{-1}$); about 98% of it being channeled through the vertical sinking of large detritus. Transport of DOM explains 23.3% ($5 \times 10^{10}$ mol N yr$^{-1}$ or $9 \times 10^{-3}$ mol N m$^{-3}$ yr$^{-1}$) of N total export, and transport of POM 9.3% ($2 \times 10^{10}$ mol N yr$^{-1}$ or $3.6 \times 10^{-3}$ mol N m$^{-3}$ yr$^{-1}$). Using a 3-D idealized coastal upwelling ecosystem, Lathuilière et al. (2010) found that 19% (497 mol N m$^{-1}$ d$^{-1}$,





BGD
8, 3537–3618, 2011



corresponding to $11 \times 10^{-3}$ mol N m$^{-3}$ yr$^{-1}$ using a 300-km wide coastal band and 55-m depth) of total export in a coastal transition zone was due to POM transport, 25% (654 mol N m$^{-1}$ d$^{-1}$ or $14.47 \times 10^{-3}$ mol N m$^{-3}$ yr$^{-1}$) to DOM transport, and 56% (1496 mol N m$^{-1}$ d$^{-1}$ or $33.09 \times 10^{-3}$ mol N m$^{-3}$ yr$^{-1}$) to POM sedimentation. Results from our realistic model of the Namibian upwelling system are coherent with estimations from Lathuilière et al. (2010).

Monteiro (2010), using a simplified representation (a box model), estimated the total annual carbon export flux in the Northern Benguela system as the sum of the vertical export of POC ($2 \times 10^{13}$ g C yr$^{-1}$ or $1.1 \times 10^{2}$ g C m$^{-2}$ yr$^{-1}$, 77% of total carbon export) and the offshore advection of dissolved organic carbon (DOC) ($0.6 \times 10^{13}$ g C yr$^{-1}$ or $0.3 \times 10^{2}$ g C m$^{-2}$ yr$^{-1}$, 23% of total carbon export). In our study, using the same definition as Monteiro (2010), the total simulated annual carbon export flux over the continental shelf and the slope off Walvis Bay area represents $1.8 \times 10^{13}$ g C yr$^{-1}$ ($3.1 \times 10^{2}$ g C m$^{-2}$ yr$^{-1}$): vertical sinking of POC out of the surface layer is equal to $1.2 \times 10^{13}$ g C yr$^{-1}$ or $2 \times 10^{2}$ g C m$^{-2}$ yr$^{-1}$ (65.7% of total carbon export), and offshore advection of DOC is $0.6 \times 10^{13}$ g C yr$^{-1}$ or $1.1 \times 10^{2}$ g C m$^{-2}$ yr$^{-1}$ (34.3% of total carbon export). Monteiro (2010) estimated annual sedimentation fluxes of POC in the Northern Benguela system sediments and found $0.7 \times 10^{13}$ g C yr$^{-1}$ (or $0.4 \times 10^{2}$ g C m$^{-2}$ yr$^{-1}$). Here, simulated sedimentation flux of POC is $0.4 \times 10^{13}$ g C yr$^{-1}$, corresponding to $0.7 \times 10^{2}$ g C m$^{-2}$ yr$^{-1}$. Our results are then in agreement with those obtained by Monteiro (2010).

The Walvis Bay area can be a non-negligible N source for the eastern part of the South Atlantic Subtropical Gyre. Using our coupled model, a N input of $28.7 \times 10^{10}$ mol N yr$^{-1}$ can be inferred at 10° E (western boundary of the entire Walvis Bay domain), between 22° S and 24° S, for the first 100 m of the water column. Assuming a horizontal surface for the South Atlantic Subtropical Gyre ($7.7 \times 10^{6}$ km$^{2}$) equivalent as the one considered in Charria et al. (2008b) for the North Atlantic Ocean, this estimation is equivalent to 0.037 mol N m$^{-2}$ yr$^{-1}$ for the entire Walvis Bay domain ($10.3 \times 10^{4}$ km$^{2}$). Assuming the same contribution for the entire BUS (18° S to 35° S





BGD
8, 3537–3618, 2011



with 10° offshore, or $10.5 \times 10^5$ km$^2$) as the entire Walvis Bay domain, the N source for the Subtropical Gyre corresponds to 0.38 mol N m$^{-2}$ yr$^{-1}$. This extrapolation certainly represents an overestimation as the Walvis Bay area is a very productive area compared to the entire BUS. This last estimation has the same order of magnitude than the other possible N sources reminded in the introduction, ranging from 0.01 to 0.24 mol N m$^{-2}$ yr$^{-1}$ (Charria et al., 2008b). As explained in the previous Sect. 5.3, fixed inorganic N loss due to denitrification and anammox is underestimated in our estimated offshore N source from the Walvis Bay area for the eastern part of the South Atlantic Subtropical Gyre. Indeed, denitrification and anammox processes occur mainly very close to the coast and in the sediment. Sediment processes are not taken into account: theses processes are mainly $O_2$ and $NO_3$ consumptions, and fixed inorganic N loss by denitrification. Moreover, the resolution of our coupled model is not fine enough on the continental shelf to really resolve biogeochemical processes very close to the coast.

### 5.5 Air-sea $N_2O$ flux

Ocean-atmosphere $N_2O$ fluxes were estimated to be equal to $+2.9 \times 10^8$ mol $N_2O$ yr$^{-1}$ in the coastal domain and $+2.6 \times 10^8$ mol $N_2O$ yr$^{-1}$ over the slope (Fig. 19). Figure 20 presents the annual mean $N_2O$ flux at the ocean-atmosphere interface using the atmospheric convention (positive flux means an outgasing of $N_2O$ from the ocean to the atmosphere). Fluxes are averaged in latitude over the same domain as the N budget (22° S to 24° S). In the open ocean, air-sea fluxes are weakly positive ($+0.8 \times 10^{-2}$ mmol $N_2O$ m$^{-2}$ d$^{-1}$). During AMT 12 (May–June 2003) and AMT 13 (September–October 2003) cruises, air-sea $N_2O$ fluxes were estimated over the South Atlantic Subtropical Gyre. Using Wanninkhof (1992) relationships, air-sea fluxes were $+1.3 \times 10^{-3}$ and $+0.4 \times 10^{-3}$ mmol $N_2O$ m$^{-2}$ d$^{-1}$ in austral autumn and spring, respectively (Robinson et al., 2006; Forster et al., 2009). Simulated air-sea $N_2O$ fluxes offshore, over the most western part of our studied domain, are higher than those estimated from in-situ measurements during AMT 12 and 13 cruises. However, the track





BGD
8, 3537–3618, 2011



of both cruises was in the oligotrophic gyre (10° S to 30° S–25° W; see the tracks on Fig. 1 from Robinson et al., 2006). Even at the most western part of our domain (5° E), conditions are not oligotrophic. Annual mean of the simulated $N_2O$ fluxes increases up to $+7 \times 10^{-2}$ mmol $N_2O$ m$^{-2}$ d$^{-1}$ close to the Namibian coast (Fig. 20). Using $N_2O$ concentrations from the FRS Africana cruise in December 2009, we estimated air-sea $N_2O$ fluxes along the Walvis Bay transect (23° S). Some assumptions were made. First, concentrations measured at the first bottle (between 4 and 18-m depth) are assumed to be representative of surface conditions. Secondly, the same formulation than the one in BioBUS (see Appendix A) is used to estimate air-sea $N_2O$ fluxes. Thirdly, we used the same wind speeds (for December) than those used to force the coupled model, deduced from the QuikSCAT monthly climatology. Estimated air-sea $N_2O$ fluxes from FRS Africana data are overlaid on Fig. 20. The three estimations made at 13.2° E ($+2.4 \pm 0.7 \times 10^{-2}$ mmol $N_2O$ m$^{-2}$ d$^{-1}$), 13.7° E ($+3 \pm 0.4 \times 10^{-2}$ mmol $N_2O$ m$^{-2}$ d$^{-1}$) and 14.1° E ($+3.6 \pm 0.6 \times 10^{-2}$ mmol $N_2O$ m$^{-2}$ d$^{-1}$) are in good agreement with the simulated fluxes. Close to the coast, air-sea $N_2O$ flux from in-situ observations can not be estimated because of an important standard deviation for the $N_2O$ concentrations measured in the water column at 14.3° E (see Sect. 4.5). Taking a mean value between the four measurements made in the first 20-m depth at 14.3° E, air-sea $N_2O$ flux is estimated at $+16.8 \times 10^{-2}$ mmol $N_2O$ m$^{-2}$ d$^{-1}$. Close to the coast, the simulated air-sea $N_2O$ flux reaches a maximum value of $+7 \times 10^{-2}$ mmol $N_2O$ m$^{-2}$ d$^{-1}$, which is less intense than the in-situ estimated one. However, this later has to be taken with caution due to high standard deviations and the mean value taken over the first 20-m depth. So, simulated air-sea $N_2O$ fluxes in the Walvis Bay area, using our coupled model, seem in reasonable agreement with estimations made with $N_2O$ data from the FRS Africana cruise in December 2009, except close to the coast. However, it is obvious that more in-situ data are needed to conclude.

As a few in-situ data are available in our studied area, we also perform comparisons with other EBUS. Four cruises and one year of monitoring off Chile provided data for determining air-sea $N_2O$ exchanges (Paulmier et al., 2008). At the fixed station





BGD
8, 3537–3618, 2011



located on the continental shelf (67-m depth), estimated air-sea $N_2O$ fluxes show great temporal variability (between September 2000 and December 2001). Values between $-1.8 \times 10^{-3}$ and $+0.33$ mmol $N_2O$ m$^{-2}$ d$^{-1}$ have been recorded during relaxation and upwelling events, respectively. The average annual $N_2O$ flux estimated at this station is $+4.5 \times 10^{-2}$ mmol $N_2O$ m$^{-2}$ d$^{-1}$. Other estimations made during cruises give an average annual $N_2O$ flux of $+6 \times 10^{-2}$ mmol $N_2O$ m$^{-2}$ d$^{-1}$ (Paulmier et al., 2008). Wittke et al. (2010) estimated $N_2O$ emissions in the Mauritanian upwelling system using a simple upwelling model, in-situ $N_2O$ measurements and QuikSCAT product. Air-sea $N_2O$ fluxes are estimated up to $+17 \times 10^{-2}$ mmol $N_2O$ m$^{-2}$ d$^{-1}$ in the northern part of the upwelling area off Mauritania, while they do not exceed $+9 \times 10^{-2}$ mmol $N_2O$ m$^{-2}$ d$^{-1}$ in the southern part. $N_2O$ emissions highlight an important seasonality driven by the wind-driven upwelling off Mauritania. Using satellite and ocean observations, and an empirical formulation adapted for the Californian coast, Lueker et al. (2003) estimated air-sea $N_2O$ fluxes of $+11 \times 10^{-2}$ mmol $N_2O$ m$^{-2}$ d$^{-1}$ during upwelling conditions. Coastal air-sea $N_2O$ fluxes estimated in our study seem in agreement with these different estimations obtained for other EBUS.

We now compare the mean simulated $N_2O$ emissions off Walvis Bay area with estimations made in other coastal upwelling regions. As coastal upwelling areas studied in Nevison et al. (2004) do not extend more than 100 km offshore, we just use the mean $N_2O$ emissions of the coastal domain off Walvis Bay (22° S to 24° S; from the coast to 200-m isobath, so around 100 km offshore) to be coherent for this comparison. For the coastal domain off Walvis Bay ($2.1 \times 10^4$ km$^2$), ocean-atmosphere $N_2O$ fluxes were estimated to be $+2.9 \times 10^8$ mol $N_2O$ yr$^{-1}$ (Fig. 19) or $+8.1$ Gg N yr$^{-1}$. This small domain does not represent more than 1.2% of the world's major eastern boundary regions ($1.75 \times 10^6$ km$^2$; Nevison et al., 2004), however its $N_2O$ emissions contribute to 4% of the emissions in the eastern boundary regions ($+200 \pm 0.140$ Gg N yr$^{-1}$; Nevison et al., 2004), and to 0.2% of the global ocean emission ($+3.8$ Tg N yr$^{-1}$; Nevison et al., 2003, 2004). For comparison, Nevison et al. (2004) estimated $+16$ Gg N yr$^{-1}$ (8% of the global $N_2O$ upwelling emissions) for the South-West Africa area (5° S–30° S:





BGD
8, 3537–3618, 2011



$1.9 \times 10^5$ km$^2$, or 10.9% of the global coastal upwelling). Dividing by the surface of each area, the coastal domain off Walvis Bay ($2.1 \times 10^4$ km$^2$) studied here emits $38.5 \times 10^{-2}$ g N m$^{-2}$ yr$^{-1}$, while the South-West Africa area ($1.9 \times 10^5$ km$^2$) from Nevison et al. (2004) emits $8.4 \times 10^{-2}$ g N m$^{-2}$ yr$^{-1}$. Other coastal upwelling areas (see Table 2 from Nevison et al., 2004) emit between 6.3 and $16.4 \times 10^{-2}$ g N m$^{-2}$ yr$^{-1}$. However, as mentioned by Wittke et al. (2010), Nevison et al. (2004) overestimate the air-sea $N_2O$ fluxes due to the gas transfer velocity and the empirical relationships used in their study. As we used the same gas transfer velocity from Wanninkhof (1992) than Nevison et al. (2004), even if the relationships used for the gas exchange overestimates the air-sea $N_2O$ fluxes, the Walvis Bay area stays an important area of emission as compared to other coastal upwellings. Therefore, even if the Walvis Bay area only contributes to 1.2% of the world's major eastern boundary regions, its $N_2O$ emissions are noticeable for these regions.

## 6 Conclusions

A coupled physical/biogeochemical model (ROMS/BioBUS) has been developed for the Namibian upwelling system. It takes into account the main planktonic communities and their specificities, a detailed description of the microbial loop, small and large particulate compartments, a DON compartment, and an oxygen equation for oxygen-dependent microbial processes. A simple module has been used to estimate the $N_2O$ production and calculate the $N_2O$ fluxes at the air-sea interface. Simulated fields were compared with different types of data available in the studied area. The model correctly represents the climatological fields as compared with CARS databases (2006 and 2009) and WOA climatology (2001; Conkright et al., 2002). Our climatological configuration obviously underestimates the important interannual variability of the Namibian upwelling system that is observed in-situ data. In future works, the coupled physical/biogeochemical model will be run using the interannual forcing to catch this interannual variability. Vertical gradients of simulated fields give satisfying results,





BGD
8, 3537–3618, 2011



except oxygen concentrations near the water-sediment interface over the continental shelf. This problem will be resolved by the addition of a sediment module that will take into account oxygen consumption by degradation processes at the water-sediment interface. Along the Namibian continental shelf, degradation of OM in the upper sediments is very active since an important part of OM falls within the water column and accumulates in the upper sediments before being remineralized.

This coupled model allowed us to estimate the N transfers from the coast to the open ocean, the N export under the surface layer, and the nitrogen ($N_2O$) exchange at the ocean-atmosphere interface in the Namibian upwelling system, and more especially in the Walvis Bay area (between 22° S and 24° S). In the surface layer (0–100 m) of the coastal and slope sub-domains, primary production is sustained by advection of nitrates: mainly by horizontal advection in the coastal domain, and mainly by upwelling in the slope domain. Over the coastal domain (0–100 m), 32.4% of total OM export is due to DOM export ($3.4 \times 10^{10}$ mol N yr$^{-1}$), 18.1% due to POM export ($1.9 \times 10^{10}$ mol N yr$^{-1}$), and 49.5% due to vertical sinking of POM below 100-m depth ($5.2 \times 10^{10}$ mol N yr$^{-1}$). The slope also represents a net loss of fixed inorganic N, advection processes export 14.4% of DOM ($1.6 \times 10^{10}$ mol N yr$^{-1}$), 1.8% is exported by advection in form of POM ($0.2 \times 10^{10}$ mol N yr$^{-1}$), and vertical sinking of POM contributes to 83.8% ($9.3 \times 10^{10}$ mol N yr$^{-1}$). Denitrification and anammox processes take place in the intermediate layer (between 100 and 600-m depth) over the continental shelf and slope. These anoxic processes contribute to the loss of fixed inorganic N ($2.2 \times 10^{8}$ mol N yr$^{-1}$) over the continental shelf and the slope. This flux is relatively weak compared to other horizontal, vertical and biogeochemical fluxes, including the air-sea $N_2O$ fluxes. However, since the $O_2$ is not yet well represented near the bottom of the water column, the biogeochemical fixed inorganic N loss could be greatly underestimated, suggesting the importance of including a sediment module to represent the biogeochemistry of this wide shelf Namibian system. Indeed, an important quantity of OM is sequestrated in the upper sediments of the Walvis Bay area. 78.8% ($4.1 \times 10^{10}$ mol N yr$^{-1}$) of POM sinking vertically at 100-m depth is sequestrated on the





BGD
8, 3537–3618, 2011



shelf sediment while only 14% ($1.3 \times 10^{10}$ mol N yr$^{-1}$, mainly above 600-m depth) of POM reaches the sediment without being remineralized on the slope. As compared with previous studies (Monteiro, 2010; Lathuilière et al., 2010), our modeling experiment provides similar results.

The N export at 10° E is non-negligible ($28.7 \times 10^{10}$ mol N yr$^{-1}$) for the first 100-m depth. An extrapolation to the entire BUS would imply a significant contribution of the upwelling region for sustaining primary production in the Subtropical Gyre. In a future work, the estimation will be made using a configuration of the entire BUS.

The Walvis Bay area is also an area where $N_2O$ is outgazed to the atmosphere. Estimated fluxes in our study have the same order of magnitude than fluxes estimated off Walvis Bay during the FRS Africana cruise in December 2009, and fluxes estimated in other EBUS. The coastal domain off Walvis Bay considered in our study does not represent more than 1.2% of the global coastal upwelling, however a simple parameterization shows that its $N_2O$ emissions (8.1 Gg N yr$^{-1}$) could contribute to 4% of the global $N_2O$ upwelling emissions, and to 0.2% of global ocean $N_2O$ emission. So, estimated emissions off Walvis Bay represent a significant area of $N_2O$ emissions for the South-West Africa region, and compared with other coastal upwelling areas. The $N_2O$ oceanic cycle deserves to be studied and better understood. Its parameterization in global models has to be improved in order to better estimate the response of the global ocean to present and future climatic changes, taking into account oxygen minimum zones, especially in Eastern Boundary Upwelling Systems.

In future works, ameliorations will be made in BioBUS to improve the microbial loop and better estimate the fixed inorganic N loss due to denitrification and anammox processes, and the $N_2O$ production in suboxic conditions. In order to better simulate very low $O_2$ concentrations on the continental shelf and fixed inorganic N loss by denitrification, a sediment module will be added to BioBUS. In this area where suboxic conditions are frequent, the $N_2O$ parameterization has to take into account $N_2O$ formation process associated with suboxic processes. The parameterization from Freing et al. (2009) will probably improve results for the $N_2O$ distribution in the OMZ. Finally, microbial





BGD
8, 3537–3618, 2011



processes, with a coupling between aerobic and anaerobic $NH_4^+$ oxidation, could be of interest to better quantify the anammox process in the BioBUS model. More studies are needed to better understand the N cycle in OMZ and improve the representation of the associated processes in coupled physical/biogeochemical models.

## Appendix A

### Formulation of the Source-Minus-Sink (SMS) terms of the BioBUS model

The model contains 12 state variables (Table 1). The formulation of the SMS terms for each of the biogeochemical tracers, with parameter values (Table 2), is given by:

$$\mathrm{SMS}(P_S)=(1-\varepsilon_{P_S})\cdot J_{P_S}(\mathrm{PAR},T,\mathrm{N})\cdot[P_S]-G_{Z_S}^{P_S}\cdot[Z_S]-G_{Z_L}^{P_S}\cdot[Z_L]-\mu_{P_S}\cdot[P_S] \quad \text{(A1)}$$

$$\mathrm{SMS}(P_L)=(1-\varepsilon_{P_L})\cdot J_{P_L}(\mathrm{PAR},T,\mathrm{N})\cdot[P_L]-G_{Z_S}^{P_L}\cdot[Z_S]-G_{Z_L}^{P_L}\cdot[Z_L]-\mu_{P_L}\cdot[P_L]+L_{VS} \quad \text{(A2)}$$

$$\mathrm{SMS}(Z_S)=f1_{Z_S}\cdot(G_{Z_S}^{P_S}+G_{Z_S}^{P_L})\cdot[Z_S]-G_{Z_L}^{Z_S}\cdot[Z_L]-\gamma_{Z_S}\cdot[Z_S]-\mu_{Z_S}\cdot[Z_S]^2 \quad \text{(A3)}$$

$$\mathrm{SMS}(Z_L)=f1_{Z_L}\cdot(G_{Z_L}^{P_S}+G_{Z_L}^{P_L}+G_{Z_L}^{Z_S})\cdot[Z_L]-\gamma_{Z_L}\cdot[Z_L]-\mu_{Z_L}\cdot[Z_L]^2 \quad \text{(A4)}$$

$$\mathrm{SMS}(D_S)=(1-f1_{Z_S})\cdot(G_{Z_S}^{P_S}+G_{Z_S}^{P_L})\cdot[Z_S]+\mu_{P_S}\cdot[P_S]+\mu_{P_L}\cdot[P_L]+\mu_{Z_S}\cdot[Z_S]^2 -\mu_{D_S}\cdot[D_S]-\mathrm{remD_S}+L_{VS} \quad \text{(A5)}$$

$$\mathrm{SMS}(D_L)=(1-f1_{Z_L})\cdot(G_{Z_L}^{P_S}+G_{Z_L}^{P_L}+G_{Z_L}^{Z_S})\cdot[Z_L]+\mu_{Z_L}\cdot[Z_L]^2-\mu_{D_L}\cdot[D_L]-\mathrm{remD_L}+L_{VS} \quad \text{(A6)}$$

$$\mathrm{SMS}(\mathrm{DON})=\varepsilon_{P_S}\cdot J_{P_S}(\mathrm{PAR},T,\mathrm{N})\cdot[P_S]+\varepsilon_{P_L}\cdot J_{P_L}(\mathrm{PAR},T,\mathrm{N})\cdot[P_L]+f2_{Z_S}\cdot\gamma_{Z_S}\cdot[Z_S] +f2_{Z_L}\cdot\gamma_{Z_L}\cdot[Z_L]+\mu_{D_S}\cdot[D_S]+\mu_{D_L}\cdot[D_L]-\mathrm{remDON} \quad \text{(A7)}$$





BGD
8, 3537–3618, 2011



$$\mathrm{SMS}(\mathrm{NO_3}) = -\left[aJ_{\mathrm{P_S}}(\mathrm{PAR},T)\cdot f'_{\mathrm{P_S}}(\mathrm{NO_3},\mathrm{NO_2})\cdot[\mathrm{P_S}] + aJ_{\mathrm{P_L}}(\mathrm{PAR},T)\cdot f'_{\mathrm{P_L}}(\mathrm{NO_3},\mathrm{NO_2})\cdot[\mathrm{P_L}]\right] \cdot \frac{[\mathrm{NO_3}]}{[\mathrm{NO_3}]+[\mathrm{NO_2}]} + \mathrm{Nitrif2} - \mathrm{Denitr1} \quad \text{(A8)}$$

$$\mathrm{SMS}(\mathrm{NO_2}) = -\left[aJ_{\mathrm{P_S}}(\mathrm{PAR},T)\cdot f'_{\mathrm{P_S}}(\mathrm{NO_3},\mathrm{NO_2})\cdot[\mathrm{P_S}] + aJ_{\mathrm{P_L}}(\mathrm{PAR},T)\cdot f'_{\mathrm{P_L}}(\mathrm{NO_3},\mathrm{NO_2})\cdot[\mathrm{P_L}]\right] \cdot \frac{[\mathrm{NO_2}]}{[\mathrm{NO_3}]+[\mathrm{NO_2}]} + \mathrm{Nitrif1} - \mathrm{Nitrif2} + \mathrm{Denitr1} - \mathrm{Denitr2} - \mathrm{Anammox} \quad \text{(A9)}$$

$$\begin{aligned}\mathrm{SMS}(\mathrm{NH_4}) = {} & -aJ_{\mathrm{P_S}}(\mathrm{PAR},T)\cdot f''_{\mathrm{P_S}}(\mathrm{NH_4})\cdot[\mathrm{P_S}] - aJ_{\mathrm{P_L}}(\mathrm{PAR},T)\cdot f''_{\mathrm{P_L}}(\mathrm{NH_4})\cdot[\mathrm{P_L}] \\ & + (1-f2_{\mathrm{Z_S}})\cdot\gamma_{\mathrm{Z_S}}\cdot[\mathrm{Z_S}] + (1-f2_{\mathrm{Z_L}})\cdot\gamma_{\mathrm{Z_L}}\cdot[\mathrm{Z_L}] \\ & - \mathrm{Nitrif1} + \mathrm{remD_S} + \mathrm{remD_L} + \mathrm{remDON} - \mathrm{Anammox}\end{aligned} \quad \text{(A10)}$$

$$\begin{aligned}\mathrm{SMS}(\mathrm{O_2}) = {} & R_{\mathrm{O_2/N}}\cdot\Big(J_{\mathrm{P_S}}(\mathrm{PAR},T,\mathrm{N})\cdot[\mathrm{P_S}] + J_{\mathrm{P_L}}(\mathrm{PAR},T,\mathrm{N})\cdot[\mathrm{P_L}] - \mathrm{DcDON}(\mathrm{O_2}) \\ & - \mathrm{DcD_S}(\mathrm{O_2}) - \mathrm{DcD_L}(\mathrm{O_2}) - (1-f2_{\mathrm{Z_S}})\cdot\gamma_{\mathrm{Z_S}}\cdot[\mathrm{Z_S}] - (1-f2_{\mathrm{Z_L}})\cdot\gamma_{\mathrm{Z_L}}\cdot[\mathrm{Z_L}]\Big) \\ & - 1{,}5\cdot\mathrm{Nitrif1} - 0{,}5\cdot\mathrm{Nitrif2} + \mathrm{FluxOA}(\mathrm{O_2})\end{aligned} \quad \text{(A11)}$$

If $[\mathrm{O_2}] > 4\ \mathrm{mmol\,O_2\,m^{-3}}$ and depth ($Z$, in meters) > depth of euphotic zone (Nevison et al., 2003):

$$\mathrm{SMS}(\mathrm{N_2O}) = R_{\mathrm{N/O_2}}(a_1/[\mathrm{O_2}]+a_2)\cdot\exp(-Z/Z_{\mathrm{scale}})\cdot(1{,}5\cdot\mathrm{Nitrif1} + 0{,}5\cdot\mathrm{Nitrif2}) \quad \text{(A12)}$$

$L_{\mathrm{VS}}$ is the sinking term which represents the sinking velocity $w_{\mathrm{P_L}}$, $w_{\mathrm{D_S}}$, or $w_{\mathrm{D_L}}$ for large phytoplankton, small and large detritus, respectively, depending of the considered equation.





BGD
8, 3537–3618, 2011



## A1 Primary production

The growth rate $J_{P_i}(\mathrm{PAR},T,\mathrm{N})$ of phytoplankton $P_i$ ($i$ represents flagellates or diatoms), is limited by light availability for photosynthesis (PAR: Photosynthetically Active Radiation), temperature $T$ (°C), and nutrients (N represents $NO_3$, $NO_2$, and $NH_4$),

$$J_{P_i}(\mathrm{PAR},T,\mathrm{N}) = aJ_{P_i}(\mathrm{PAR},T)\cdot f_{P_i}(\mathrm{NO_3},\mathrm{NO_2},\mathrm{NH_4}) \quad \text{(A13)}$$

$aJ_{P_i}$ (PAR,$T$) represents the phytoplankton $P_i$ growth rate limitation by PAR and temperature, using the analytical formulation of Evans and Parslow (1985):

$$aJ_{P_i}(\mathrm{PAR},T) = \frac{J\max_{P_i}\cdot\alpha_{P_i}\cdot\mathrm{PAR}}{\sqrt{(J\max_{P_i}^2+(\alpha_{P_i}\cdot\mathrm{PAR})^2)}} \quad \text{(A14)}$$

where $J\max_{P_i}$ is the maximal light-saturated growth rate, function of temperature (Eppley, 1972):

$$J\max_{P_i} = a_{P_i}\cdot b^{c\cdot T} \quad \text{(A15)}$$

Exponential decrease of light intensity is formulated as in Koné et al. (2005):

$$\mathrm{PAR}(z) = \mathrm{PAR}_0\cdot\exp\left(-\left(k_w\cdot z + k_{\text{chl-}a}\cdot\int_z^0\theta\cdot R_{\mathrm{C/N}}\cdot[P_t]\cdot\Delta z\right)\right) \quad \text{(A16)}$$

$\mathrm{PAR}_0$ is the incident radiation at the surface of the ocean, $k_w$ and $k_{\mathrm{Chl}}$ are the light attenuation coefficients due to water and to chlorophyll-$a$, respectively. $\theta$ is the chlorophyll/carbon ratio, $r_{\mathrm{C/N}}$ is the carbon/nitrogen Redfield ratio for phytoplankton, [$P_t$] represents the sum of nano- and microphytoplankton concentrations, $\Delta z$ is the depth step (vertical thickness) (m).

Limitation by nutrients (Fasham et al., 1990) is given by a Michaelis-Menten formulation:

$$f_{P_i}(\mathrm{NO_3},\mathrm{NO_2},\mathrm{NH_4}) = f'_{P_i}(\mathrm{NO_3},\mathrm{NO_2}) + f''_{P_i}(\mathrm{NH_4})$$





BGD
8, 3537–3618, 2011



$$f_{P_i}(NO_3, NO_2, NH_4) = \frac{([NO_3]+[NO_2])\cdot \exp(-K_{psi}\cdot[NH_4])}{K_{NO_{3P_i}}+[NO_3]+[NO_2]} + \frac{[NH_4]}{K_{NH_{4P_i}}+[NH_4]} \quad \text{(A17)}$$

The phytoplankton $P_i$ growth rate is limited by $NO_3$, $NO_2$, and $NH_4$. $NH_4$ is preferred to $NO_3$ and $NO_2$ for phytoplankton. $K_{NO_{3P_i}}$ and $K_{NH_{4P_i}}$ are the half-saturation constants for $NO_3 + NO_2$ and $NH_4$ uptakes by flagellates or diatoms. Small phytoplankton cells are more adapted to low nutrient and stratified conditions than larger ones. Half-saturation constants for $NO_3$ and $NO_2$ are usually higher than those for $NH_4$, for both flagellates and diatoms (Eppley et al., 1969; Caperon and Meyer, 1972a, b). Besides the more elevated surface/volume ratio, small cells have better assimilation efficiency than large cells (Nalewajko and Garside, 1983). So, the half-saturation constants are lower for flagellates than diatoms.

Note that here, it is assumed that phytoplankton are no limited by phosphate (Dittmar and Birkicht, 2001; Tyrrell and Lucas, 2002) and/or silicate and/or other micro-nutrient like metals (e.g. Fe), which is reasonable for the Namibian upwelling system.

## A2 Grazing

The specific feeding rate of a predator $Z_j$ on a food type $P_i$ is calculated according to the following formulation (Tian et al., 2000, 2001):

$$G_{Z_j}^{P_i} = g_{\max_{Z_j}} \cdot \frac{e_{Z_jP_i}\cdot[P_i]}{k_{Z_j}+F_t}, \quad \text{avec} \quad F_t = \sum e_{Z_jP_i}\cdot[P_i] \quad \text{(A18)}$$

$g_{\max_{Z_j}}$ is the maximum grazing rate of the predator $Z_j$ ($j$ represents ciliates or copepods), $e_{Z_jP_i}$ is the preference of the predator $Z_j$ to the prey $P_i$, $[P_i]$ is the prey concentration, $k_{Z_j}$ is the half-saturation constant of the predator $Z_j$ for ingestion, $F_t$ is the total biomass of available food for the predator $Z_j$ (Fasham et al., 1999).





BGD
8, 3537–3618, 2011



### A3 Remineralization of particulate and dissolved detritus

Decomposition of detritus ($D_S$ or $D_L$) or dissolved organic nitrogen DON (named Det in the following equations), is formulated as follow (Yakushev et al., 2007):

$$\text{remDet} = \text{DcDet}(O_2) + \text{DcDet}(NO_3) \quad \text{(A19)}$$

$\text{DcDet}(O_2)$ is the decomposition of Det in oxic conditions:

$$\text{DcDet}(O_2) = \exp(K\text{tox} \cdot T) \cdot K_N \cdot [\text{Det}] \cdot F\text{ox} \quad \text{(A20)}$$

$$\text{If } [O_2] \le O_2\text{ox} \text{ then: } F\text{ox} = 0$$

$$\text{If } [O_2] > O_2\text{ox} \text{ then: } F\text{ox} = ([O_2]-O_2\text{ox})/([O_2]-O_2\text{ox}+K\text{ox})$$

where $K_N$ is the remineralization rate in oxic conditions ($K_{NP4}$ for $D_S$ and $D_L$, and $K_{ND4}$ for the DON).

$\text{DcDet}(NO_3)$ is the decomposition of Det in suboxic conditions (denitrification):

$$\text{DcDet}(NO_3)=0.5\cdot\text{Denitr1}(\text{Det})+0.75\cdot\text{Denitr2}(\text{Det}) \quad \text{(A21)}$$

$$\text{Denitr1}(\text{Det})=K_{N32}\cdot F\text{dnox}\cdot F\text{dn}NO_3\cdot[\text{Det}] \quad \text{(A22)}$$

$$\text{Denitr2}(\text{Det}) = K_{N24} \cdot F\text{dnox} \cdot F\text{dn}NO_2 \cdot [\text{Det}]$$

$$\text{If } [O_2] > O_2\text{dn} \text{ then: } F\text{dnox} = 0$$

$$\text{If } [O_2] \le O_2\text{dn} \text{ then: } F\text{dnox} = 1 - [O_2]/(O_2\text{dn} \cdot (O_2\text{dn}+1-[O_2]))$$

$$\text{If } [NO_3] \le NO_3\text{mi} \text{ then: } F\text{dn}NO_3 = 0$$

$$\text{If } [NO_3] > NO_3\text{mi} \text{ then: } F\text{dn}NO_3 = ([NO_3]-NO_3\text{mi})/([NO_3]-NO_3\text{mi}+1)$$

$$\text{If } [NO_2] \le NO_2\text{mi} \text{ then: } F\text{dn}NO_2 = 0$$

$$\text{If } [NO_2] > NO_2\text{mi} \text{ then: } F\text{dn}NO_2 = ([NO_2]-NO_2\text{mi})/([NO_2]-NO_2\text{mi}+1) \quad \text{(A23)}$$





BGD
8, 3537–3618, 2011



Then, the 1st and 2nd stages of denitrification are:

$$\text{Denitr1} = \text{Denitr1}(\text{DON}) + \text{Denitr1}(D_S) + \text{Denitr1}(D_L) \quad \text{(A24)}$$

$$\text{Denitr2} = \text{Denitr2}(\text{DON}) + \text{Denitr2}(D_S) + \text{Denitr2}(D_L) \quad \text{(A25)}$$

### A4 Nitrification (Yakushev et al., 2007)

$$\text{1st stage of nitrification } (NH_4 \rightarrow NO_2): \ \text{Nitrif1} = \frac{K_{N42} \cdot [O_2]}{[O_2] + O_2\text{nf}} \cdot [NH_4] \quad \text{(A26)}$$

$$\text{2nd stage of nitrification } (NO_2 \rightarrow NO_3): \ \text{Nitrif2} = \frac{K_{N23} \cdot [O_2]}{[O_2] + O_2\text{nf}} \cdot [NO_2] \quad \text{(A27)}$$

### A5 Anammox (Yakushev et al., 2007)

$$\text{Anammox} = K_{\text{anammox}} \cdot [NO_2] \cdot [NH_4] \cdot K_{\text{convert}} \quad \text{(A28)}$$

### A6 Fluxes at the ocean-atmosphere interface

$O_2$ and $N_2O$ fluxes at the ocean-atmosphere interface are expressed using the gas transfer velocity from Wanninkhof (1992), and the Schmidt number from Keeling et al. (1998) for $O_2$ and from Wanninkhof (1992) for $N_2O$. $O_2$ saturation concentrations at one atmosphere total pressure for water-saturated air come from Garcia and Gordon (1992). $N_2O$ concentrations in equilibrium with moist air at total pressure of one atmosphere come from Weiss and Price (1980). The dry mole fraction of atmospheric $N_2O$ is assumed to be 318 ppb (Lueker et al., 2003; Cornejo et al., 2006; Anonymous, 2008).





BGD
8, 3537–3618, 2011



### A7 Chlorophyll/Nitrate ratio

Chlorophyll-*a* concentrations ([Chl-*a*]; in mg Chl $m^{-3}$) are derived from simulated phytoplankton concentrations ([P]; in mmol N $m^{-3}$) using a variable Chl/N ratio following (Hurtt and Armstrong, 1996):

$$[\text{Chl-}a] = 1{,}59 \cdot \chi \cdot [\text{P}] \quad \text{(A29)}$$

1.59 is the standard Chl/N ratio (in g Chl $(\text{mol N})^{-1}$). If growth is light limited, then the Chl/N ratio is maximum and $\chi = \chi_{max} = 1$, hence $C/Chl_{min} = 50\,g\,C\,g\,Chl^{-1}$. If phytoplankton growth is nutrient limited, $\chi$ = nutrient-limited growth rate/light-limited growth rate, and the upper limit for the $(C/Chl)_{max}$ is fixed to $160\,g\,C\,g\,Chl^{-1}$ (Charria et al., 2008b). In this case, the applied $\chi$ ratio increases with the quantity of light available for a constant growth rate.

*Acknowledgements.* We would like to thank the CNES and Midi-Pyrénées Region for the financial PhD support attributed to E. Gutknecht, and the CNES support (TOSCA CNES program) to I. Dadou and V. Garçon. The COST Action 735 is thank for the financial grant for E. Gutknecht's scientific mission effectuated at National Environmental Research Institute (Aarhus University, Roskilde, Denmark), and L. L. Sørensen (NERI, Denmark) for her welcome there and the access to Galathea data A. Silio-Calzada and A. Bricaud (LOV, France) are thank for the use of their satellite products. For the AMT data, we are grateful the BODC (British Oceanographic Data Center, UK), C. Robinson (PML/UEA, UK), R. Harris (PML, UK), T. Bale (PML, UK), M. Woodward (PML, UK), E. Fernandez (UV, Spain), R. Barlow (MCM, South Africa), P. Holligan (PML, UK), and R. Sanders (NOCS, UK) for providing their data. Ocean color data were produced by the SeaWiFS project at GSFC and obtained from the DAAC. We thank the CSIRO Marine and Atmospheric Research for the development and distribution of CARS databases (2006 and 2009) and the German Federal Ministry of Education and Research for supporting GENUS (03F0497D). We express our special thanks to V. Koné (LPO, France) for his $N_2P_2Z_2D_2$ model, P. Marchesiello (LEGOS, France) for his advices and explanations on the ROMS model, and H. Bange (IFM-GEOMAR, Germany) for his fruitful advices on the manuscript.





BGD
8, 3537–3618, 2011



The publication of this article is financed by CNRS-INSU.

## References

Aiken, J.: Atlantic Meridional Transect, AMT 6 cruise report, 14 May–16 June 1998.

Aiken, J. and Bale, A. J.: An introduction to the Atlantic Meridional Transect (AMT) Programme, Prog. Oceanogr., 45(3–4), 251–256, doi:10.1016/S0079-6611(00)00004-5, 2000.

Aiken, J., Rees, N., Hooker, S., Holligan, P., Bale, A., Robins, D., Moore, G., Harris, R., and Pilgrim, D.: The Atlantic Meridional Transect: overview and synthesis of data, Prog. Oceanogr., 45(3–4), 257–312, doi:10.1016/S0079-6611(00)00005-7, 2000.

Anonymous: Greenhouse gases hit modern day-highs, Nature, 456, 558–559, doi:10.1038/456558b, 2008.

Bange, H.: New Directions: The importance of oceanic nitrous oxide emissions, Atmos. Environ., 40(1), 198–199, doi:10.1016/j.atmosenv.2005.09.030, 2006.

Bange, H.: Gaseous nitrogen compounds (NO, $N_2O$, $N_2$, $NH_3$) in the ocean, in: Nitrogen in the Marine Environment, edited by: Capone, D. G., Bronk, D. A., Mulholland, M. R., and Carpenter, E. J., Amsterdam, 51–94, 2008.

Barlow, R. G., Aiken, J., Holligan, P. M., Cummings, D. G., Maritorena, S., and Hooker, S.: Phytoplankton pigment and absorption characteristics along meridional transects in the Atlantic Ocean, Deep-Sea Res. Pt. I, 49(4), 637–660, doi:10.1016/S0967-0637(01)00081-4, 2002.

Barlow, R. G., Aiken, J., Moore, G. F., Holligan, P. M., and Lavender, S.: Pigment adaptations in surface phytoplankton along the eastern boundary of the Atlantic Ocean, Mar. Ecol.-Prog. Ser., 281, 13–26, doi:10.3354/meps281013, 2004.

Barlow, R., Lamont, T., Mitchell-Innes, B., Lucas, M., and Thomalla, S.: Primary production in the Benguela ecosystem, 1999–2002, Afr. J. Mar. Sci., 31(1), 97–101, doi:10.2989/AJMS.2009.31.1.9.780, 2009.





BGD

8, 3537–3618, 2011



Barnier, B., Siefridt, L., and Marchesiello, P.: Thermal forcing for a global ocean circulation model using a three-year climatology of ECMWF analyses, J. Marine Syst., 6(4), 363–380, doi:10.1016/0924-7963(94)00034-9, 1995.
Boebel, O., Rossby, T., Lutjeharms, J., Zenk, W., and Barron, C.: Path and variability of the Agulhas Return Current, Deep-Sea Res. Pt. II, 50(1), 35–56, doi:10.1016/S0967-0645(02)00377-6, 2003.
Brown, P. C., Painting, S. J., and Cochrane, K. L.: Estimates of phytoplankton and bacterial biomass and production in the northern and southern Benguela ecosystems, S. Afr. J. Sci., 11, 537–564, 1991.
Caperon, J. and Meyer, J.: Nitrogen-limited growth of marine phytoplankton – I. Changes in population characteristics with steady-state growth rate, Deep-Sea Res., 19(9), 601–618, doi:10.1016/0011-7471(72)90089-7, 1972a.
Caperon, J. and Meyer, J.: Nitrogen-limited growth of marine phytoplankton – II. Uptake kinetics and their role in nutrient limited growth of phytoplankton, Deep-Sea Res., 19(9), 619–632, doi:10.1016/0011-7471(72)90090-3, 1972b.
Capet, X., Colas, F., Penven, P., Marchesiello, P., and McWilliams, J. C.: Eddies in Eastern Boundary Subtropical Upwelling Systems, in: Geophysical Monograph Series, vol. 177, Ocean Modeling in an Eddying Regime, edited by: Hecht, M. W. and Hasumi, H. H., AGU, Washington, D. C., 350 pp., 2008.
Carlson, C. A. and Ducklow, H. W.: Dissolved organic carbon in the upper ocean of the central equatorial Pacific Ocean, 1992: Daily and finescale vertical variations, Deep-Sea Res. Pt. II, 42(2–3), 639–656, doi:10.1016/0967-0645(95)00023-J, 1995.
Carr, M. E.: Estimation of potential productivity in Eastern Boundary Currents using remote sensing, Deep-Sea Res. Pt. II, 49(1–3), 59–80, 2002.
Carr, M. and Kearns, E. J.: Production regimes in four Eastern Boundary Current systems, Deep-Sea Res. Pt. II, 50(22–26), 3199–3221, doi:10.1016/j.dsr2.2003.07.015, 2003.
CARS: CSIRO Atlas of Regional Seas, http://www.marine.csiro.au/~dunn/cars2006, access: 30 March 2011, 2006.
CARS: CSIRO Atlas of Regional Seas, http://www.marine.csiro.au/~dunn/cars2009, access: 30 March 2011, 2009.
Casey, K. S. and Cornillon, P.: A comparison of satellite and in situ-based sea surface temperature climatologies, J. Climate, 12(6), 1848–1863, 1999.
Charria, G., Dadou, I., Cipollini, P., Drévillon, M., De Mey, P., and Garçon, V.: Understanding





BGD
8, 3537–3618, 2011



the influence of Rossby waves on surface chlorophyll-a concentrations in the North Atlantic Ocean, J. Mar. Res., 64(1), 43–71, 10.1357/002224006776412340, 2006.
Charria, G., Dadou, I., Llido, J., Drévillon, M., and Garçon, V.: Importance of dissolved organic nitrogen in the north Atlantic Ocean in sustaining primary production: a 3-D modelling approach, Biogeosciences, 5, 1437–1455, doi:10.5194/bg-5-1437-2008, 2008a.
Charria, G., Dadou, I., Cipollini, P., Drévillon, M., and Garçon, V.: Influence of Rossby waves on primary production from a coupled physical-biogeochemical model in the North Atlantic Ocean, Ocean Sci., 4, 199–213, doi:10.5194/os-4-199-2008, 2008b.
Chavez, F. P. and Messie, M.: A comparison of Eastern Boundary Upwelling Ecosystems, Prog. Oceanogr., 83(1–4), 80–96, doi:10.1016/j.pocean.2009.07.032, 2009.
Chavez, F. P. and Toggweiler, K.: Upwelling in the Ocean: Modern Processes and Ancient Records, John Wiley & Sons, 1995.
Codispoti, L. A.: Interesting Times for Marine $N_2O$, Science, 327, 1339–1340, doi:10.1126/science.1184945, 2010.
Codispoti, L. A., Brandes, J. A., Christensen, J. P., Devol, A. H., Naqvi, S. W. A., Paerl, H. W., and Yoshinari, T.: The oceanic fixed nitrogen and nitrous oxide budgets: Moving targets as we enter the anthropocene?, Sci. Mar., 65(S2), 85–105, doi:10.3989/scimar.2001.65s285, 2001.
Conkright, M. E. and O'Brien, T. D.: World Ocean Atlas 2001, Volume 6: Chlorophyll, Global Biogeochem. Cy., 8(1), 65–80, doi:199410.1029/93GB03318, 1994.
Conkright, M. E., O'Brien, T. D., Stephens, C., Locarnini, R. A., Garcia, H. E., Boyer, T. P., and Antonov, J. I.: World Ocean Atlas 2001, Volume 6: Chlorophyll, edited by: Levitus, S., NOAA Atlas NESDIS 52, US Government Printing Office, Wash., D.C., 2002.
Cornejo, M., Farías, L., and Paulmier, A.: Temporal variability in $N_2O$ water content and its air-sea exchange in an upwelling area off central Chile (36° S), Mar. Chem., 101(1–2), 85–94, doi:10.1016/j.marchem.2006.01.004, 2006.
Da Silva, A. M., Young, C. C., and Levitus, S.: Atlas of Surface Marine Data 1994, Vol. 1: Algorithms and Procedures, NOAA Atlas NESDIS 6, Department of Commerce, Washington, DC, USA, 1994.
Dadou, I., Lamy, F., Rabouille, C., Ruiz-Pino, D., Andersen, V., Bianchi, M., and Garcon, V.: An integrated biological pump model from the euphotic zone to the sediment: a 1-D application in the Northeast tropical Atlantic, Deep-Sea Res. Pt. II, 48(10), 2345–2381, 2001.
Dadou, I., Evans, G., and Garcon, V.: Using JGOFS in situ and ocean color data to compare





BGD
8, 3537–3618, 2011



biogeochemical models and estimate their parameters in the subtropical North Atlantic Ocean, J. Mar. Res., 62(4), 565–594, 2004.
Dalsgaard, T., Thamdrup, B., and Canfield, D. E.: Anaerobic ammonium oxidation (anammox) in the marine environment, Res. Microbiol., 156(4), 457–464, doi:10.1016/j.resmic.2005.01.011, 2005.
Debreu, L., Marchesiello, P., and Penven, P.: Two ways embedding algorithms for a split-explicit free surface model, Ocean Model., submitted, 2011.
Denman, K. L., Brasseur, G., Chidthaisong, A., Ciais, P., Cox, P. M., Dickinson, R. E., Hauglustaine, D., Heinze, C., Holland, E., Jacob, D., Lohmann, U., Ramachandran, S., da Silva Dias, P. L., Wofsy, S. C., and Zhang, X.: Couplings Between Changes in the Climate System and Biogeochemistry, in: Climate Change 2007: The Physical Science Basis. Contribution of Working Group I to the Fourth Assessment Report of the Intergovernmental Panel on Climate Change, edited by: Solomon, S., Qin, D., Manning, M., Chen, Z., Marquis, M., Averyt, K. B., Tignor, M., and Miller, H. L., Cambridge University Press, Cambridge, United Kingdom and New York, NY, USA, 2007.
Devol, A. H.: Denitrification including Anammox, in: Nitrogen in the Marine Environment, edited by: Capone, D. G., Bronk, D. A., Mulholland, M. R., and Carpenter, E. J., Amsterdam, 263–301, 2008.
Dittmar, T. and Birkicht, M.: Regeneration of nutrients in the northern Benguela upwelling and the Angola-Benguela Front areas, S. Afr. J. Sci., 97(5–6), 239–246, 2001.
Ekau, W., Auel, H., Pörtner, H.-O., and Gilbert, D.: Impacts of hypoxia on the structure and processes in pelagic communities (zooplankton, macro-invertebrates and fish), Biogeosciences, 7, 1669–1699, doi:10.5194/bg-7-1669-2010, 2010.
Eppley, R. W.: Temperature and Phytoplankton Growth in the Sea, Fish. B.–NOAA, 70(4), 1063–1085, 1972.
Eppley, R. W., Rogers, J. N., and McCarthy, J. J.: Half-Saturation Constants for Uptake of Nitrate and Ammonium by Marine Phytoplankton, Limnol. Oceanogr., 14(6), 912–920, 1969.
Evans, G. T. and Parslow, J. S.: A model of annual plankton cycles, Bio. Oceanogr., 3(3), 327–347, 1985.
Farias, L., Paulmier, A., and Gallegos, M.: Nitrous oxide and N-nutrient cycling in the oxygen minimum zone off northern Chile, Deep-Sea Res. Pt. I, 54(2), 164–180, doi:10.1016/j.dsr.2006.11.003, 2007.
Fasham, M. J. R., Ducklow, H. W., and McKelvie, S. M.: A nitrogen-based model of plankton





BGD
8, 3537–3618, 2011



dynamics in the oceanic mixed layer, J. Mar. Res., 48(3), 591–639, 1990.
Fasham, M. J. R., Boyd, P. W., and Savidge, G.: Modeling the Relative Contributions of Autotrophs and Heterotrophs to Carbon Flow at a Lagrangian JGOFS Station in the Northeast Atlantic: The Importance of DOC, Limnol. Oceanogr., 44(1), 80–94, 1999.
Forster, G., Upstill-Goddard, R. C., Gist, N., Robinson, C., Uher, G., and Woodward, E. M. S.: Nitrous oxide and methane in the Atlantic Ocean between 50° N and 52° S: Latitudinal distribution and sea-to-air flux, Deep-Sea Res. Pt. II, 56(15), 964–976, doi:10.1016/j.dsr2.2008.12.002, 2009.
Freing, A., Wallace, D. W. R., Tanhua, T., Walter, S., and Bange, H. W.: North Atlantic production of nitrous oxide in the context of changing atmospheric levels, Global Biogeochem. Cy., 23, GB4014, doi:10.1029/2009GB003472, 2009.
Garcia, H. E. and Gordon, L. I.: Oxygen Solubility in Seawater: Better Fitting Equations, Limnol. Oceanogr., 37(6), 1307–1312, 1992.
Gilbert, D., Rabalais, N. N., Díaz, R. J., and Zhang, J.: Evidence for greater oxygen decline rates in the coastal ocean than in the open ocean, Biogeosciences, 7, 2283–2296, doi:10.5194/bg-7-2283-2010, 2010.
Gutknecht E., Dadou, I., Charria, G., Cipollini, P., and Garçon, V.: Spatial and temporal variability of the remotely sensed chlorophyll-a signal associated with Rossby waves in the South Atlantic Ocean, J. Geophys. Res., 115, C05004, doi:10.1029/2009JC005291, 2010.
Holligan, P.: Atlantic Meridional Transect, AMT 17 cruise report, 15 October to 28 November 2005.
Huggett, J., Verheye, H., Escribano, R., and Fairweather, T.: Copepod biomass, size composition and production in the Southern Benguela: Spatio-temporal patterns of variation, and comparison with other eastern boundary upwelling systems, Prog. Oceanogr., 83(1–4), 197–207, doi:10.1016/j.pocean.2009.07.048, 2009.
Huret, M., Dadou, I., Dumas, F., Lazure, P., and Garcon, V.: Coupling physical and biogeochemical processes in the Rio de la Plata plume, Cont. Shelf Res., 25(5–6), 629–653, doi:10.1016/j.csr.2004.10.003, 2005.
Hurtt, G. C. and Armstrong, R. A.: A pelagic ecosystem model calibrated with BATS data, Deep-Sea Res. Pt. II, 43(2–3), 653–683, 1996.
Hutchings, L., van der Lingen, C. D., Shannon, L. J., Crawford, R. J. M., Verheye, H. M. S., Bartholomae, C. H., van der Plas, A. K., Louw, D., Kreiner, A., Ostrowski, M., Fidel, Q., Barlow, R. G., Lamont, T., Coetzee, J., Shillington, F., Veitch, J., Currie, J. C., and Monteiro,





BGD
8, 3537–3618, 2011



P. M. S.: The Benguela Current: An ecosystem of four components, Prog. Oceanogr., 83(1–4), 15–32, doi:10.1016/j.pocean.2009.07.046, 2009.
Jackett, D. R. and McDougall, T. J.: Minimal Adjustment of Hydrographic Profiles to Achieve Static Stability, J. Atmos. Ocean. Tech., 12(2), 381–389, 1995.
Jain, A. K., Briegleb, B. P., Minschwaner, K., and Wuebbles, D. J.: Radiative forcings and global warming potentials of 39 greenhouse gases, J. Geophys. Res., 105, 20773–20790, 2000.
Keeling, R. F., Stephens, B. B., Najjar, R. G., Doney, S. C., Archer, D., and Heimann, M.: Seasonal variations in the atmospheric O2/N2 ratio in relation to the kinetics of air-sea gas exchange, Global Biogeochem. Cy., 12(1), 141–163, doi:199810.1029/97GB02339, 1998.
Kirchman, D. L., Lancelot, C., Fasham, M., Legendre, L., Radach, G., and Scott, M.: Dissolved organic matter in biogeochemical models in the ocean, in: Towards a Model of Ocean Biogeochemical Processes, Springer-Verlag, 209–225, 1993.
Koné, V., Machu, E., Penven, P., Andersen, V., Garcon, V., Freon, P., and Demarcq, H.: Modeling the primary and secondary productions of the southern Benguela upwelling system: A comparative study through two biogeochemical models, Global Biogeochem. Cy., 19(4), GB4021, doi:10.1029/2004GB002427, 2005.
Kreiner, A. and Ayon, P.: Zooplankton dynamics from 1994 to 2006 in the upwelling systems off Peru and northern Namibia, Eastern boundary upwelling ecosystems, Las Palmas, Gran Canaria, Spain, 2–6 June 2008, P08_OP05, 2008.
Kuypers, M. M. M., Lavik, G., Woebken, D., Schmid, M., Fuchs, B. M., Amann, R., Jørgensen, B. B., and Jetten, M. S. M.: Massive nitrogen loss from the Benguela upwelling system through anaerobic ammonium oxidation, P. Natl. Acad. Sci. USA, 102(18), 6478–6483, doi:10.1073/pnas.0502088102, 2005.
Lacroix, G. and Nival, P.: Influence of meteorological variability on primary production dynamics in the Ligurian Sea (NW Mediterranean Sea) with a 1D hydrodynamic/biological model, J. Marine Syst., 16(1–2), 23–50, doi:10.1016/S0924-7963(97)00098-5, 1998.
Lam, P., Jensen, M. M., Lavik, G., McGinnis, D. F., Müller, B., Schubert, C. J., Amann, R., Thamdrup, B., and Kuypers, M. M. M.: Linking crenarchaeal and bacterial nitrification to anammox in the Black Sea, P. Natl. Acad. Sci. USA, 104(17), 7104–7109, doi:10.1073/pnas.0611081104, 2007.
Large, W. G., McWilliams, J. C., and Doney, S. C.: Oceanic vertical mixing: A review and a model with a nonlocal boundary layer parameterization, Rev. Geophys., 32(4), 363–403, doi:199410.1029/94RG01872, 1994.





BGD
8, 3537–3618, 2011



Lathuilière, C., Echevin, V., Lévy, M., and Madec, G.: On the role of the mesoscale circulation on an idealized coastal upwelling ecosystem, J. Geophys. Res., 115, C09018, doi:201010.1029/2009JC005827, 2010.
Lavik, G., Stuhrmann, T., Bruchert, V., Van der Plas, A., Mohrholz, V., Lam, P., Muszmann, M., Fuchs, B. M., Amann, R., Lass, U., and Kuypers, M. M. M.: Detoxification of sulphidic African shelf waters by blooming chemolithotrophs, Nature, 457, 581–584, doi:10.1038/nature07588, 2009.
Liu, W. T., Tang, W., and Polito, P. S.: NASA scatterometer provides global ocean-surface wind fields with more structures than numerical weather prediction, Geophys. Res. Lett., 25(6), 761–764, 1998.
Lueker, T. J., Walker, S. J., Vollmer, M. K., Keeling, R. F., Nevison, C. D., Weiss, R. F., and Garcia, H. E.: Coastal upwelling air-sea fluxes revealed in atmospheric observations of $O_2/N_2$, $CO_2$ and $N_2O$, Geophys. Res. Lett., 30(6), 1292, doi:10.1029/2002GL016615, 2003.
Lutjeharms, J. R. E., Boebel, O., and Rossby, H. T.: Agulhas cyclones, Deep-Sea Res. Pt. II, 50(1), 13–34, doi:10.1016/S0967-0645(02)00378-8, 2003.
Marchesiello, P., McWilliams, J. C., and Shchepetkin, A.: Open boundary conditions for long-term integration of regional oceanic models, Ocean Model., 3(1–2), 1–20, doi:10.1016/S1463-5003(00)00013-5, 2001.
Marchesiello, P., McWilliams, J. C., and Shchepetkin, A.: Equilibrium structure and dynamics of the California Current System, J. Phys. Oceanogr., 33(4), 753–783, 2003.
McClain, C. R., Cleave, M. L., Feldman, G. C., Gregg, W. W., Hooker, S. B., and Kuring, N.: Science Quality SeaWiFS Data for Global Biosphere Research, NASA/Goddard Space Flight Center, Sea Technol., 39(9), 10–16, 1998.
Mohrholz, V., Schmidt, M., Lutjeharms, J. R. E., and John, H.: Space-time behaviour of the Angola-Benguela Frontal Zone during the Benguela Niño of April 1999, Int. J. Remote Sens., 25(7), 1337–1340, doi:10.1080/01431160310001592265, 2004.
Mohrholz, V., Bartholomae, C. H., van der Plas, A. K., and Lass, H. U.: The seasonal variability of the northern Benguela undercurrent and its relation to the oxygen budget on the shelf, Cont. Shelf Res., 28(3), 424–441, doi:10.1016/j.csr.2007.10.001, 2008.
Molina, V. and Farías, L.: Aerobic ammonium oxidation in the oxycline and oxygen minimum zone of the eastern tropical South Pacific off northern Chile (~20° S), Deep-Sea Res. Pt. II, 56(16), 1032–1041, doi:10.1016/j.dsr2.2008.09.006, 2009.
Monteiro, P. M. S.: The Benguela Current System, Chap. 2: Eastern Boundary Current





BGD
8, 3537–3618, 2011



Systems, in: Carbon and Nutrient Fluxes in Continental Margins: A Global Synthesis, edited by: Liu, K.-K., Atkinson, L., Quiñones, R., and Talaue-MacManus, L., Berlin, 65–78, 2010.
Monteiro, P. M. and van der Plas, A. K.: Low oxygen water (LOW) variability in the Benguela system: Key processes and forcing scales relevant to forecasting, in Benguela – Predicting a Large Marine Ecosystem, Elsevier, 14, 71–90, 2006.
Monteiro, P. M. S., van der Plas, A., Mohrholz, V., Mabille, E., Pascall, A., and Joubert, W.: Variability of natural hypoxia and methane in a coastal upwelling system: Oceanic physics or shelf biology?, Geophys. Res. Lett., 33(16), L16614, doi:10.1029/2006GL026234, 2006.
Monteiro, P. M. S., van der Plas, A. K., Mélice, J., and Florenchie, P.: Interannual hypoxia variability in a coastal upwelling system: Ocean-shelf exchange, climate and ecosystem-state implications, Deep-Sea Res. Pt. I, 55(4), 435–450, doi:10.1016/j.dsr.2007.12.010, 2008.
Monteiro, P. M. S., Dewitte, B., Scranton, M. I., Paulmier, A., and Van der Plas, A.: The Role of Open Ocean Boundary Forcing on Seasonal to Decadal Scale Variability and Long-Term Change of Natural Shelf Hypoxia, Environ. Res. Lett., accepted, 2011.
Nalewajko, C. and Garside, C.: Methodological Problems in the Simultaneous Assessment of Photosynthesis and Nutrient Uptake in Phytoplankton as Functions of Light Intensity and Cell Size, Limnol. Oceanogr., 28(3), 591–597, 1983.
Naqvi, S. W. A., Bange, H. W., Farías, L., Monteiro, P. M. S., Scranton, M. I., and Zhang, J.: Marine hypoxia/anoxia as a source of $CH_4$ and $N_2O$, Biogeosciences, 7, 2159–2190, doi:10.5194/bg-7-2159-2010, 2010.
Nevison, C., Butler, J. H., and Elkins, J. W.: Global distribution of $N_2O$ and the Delta $N_2O$-AOU yield in the subsurface ocean, Global Biogeochem. Cy., 17(4), 1119, doi:10.1029/2003GB002068, 2003.
Nevison, C. D., Lueker, T. J., and Weiss, R. F.: Quantifying the nitrous oxide source from coastal upwelling, Global Biogeochem. Cy., 18(1), GB1018, doi:10.1029/2003GB002110, 2004.
Olivieri, R. A. and Chavez, F. P.: A model of plankton dynamics for the coastal upwelling system of Monterey Bay, California, Deep-Sea Res. Pt. II, 47(5–6), 1077–1106, doi:10.1016/S0967-0645(99)00137-X, 2000.
O'Reilly, J. E., Maritorena, S., Siegel, D., O 'Brien, M., Toole, D., Greg Mitchell, B., Kahru, M., Chavez, F., Strutton, P., Cota, G., Hooker, S., McClain, C., Carder, K., Muller-Karger, F., Harding, L., Magnuson, A., Phinney, D., Moore, G., Aiken, J., Arrigo, K., Letelier, R. and Culver, M.: Ocean color chlorophyll-a algorithms for SeaWiFS, OC2, and OC4: Version 4, in: SeaWiFS Postlaunch Calibration and Validation Analyses, Part 3. NASA Tech. Memo.





BGD
8, 3537–3618, 2011



2000-206892, Vol. 11, edited by: Hooker, S. B. and Firestone, E. R., NASA Goddard Space Flight Center, Greenbelt, Maryland, 9–23, 2000.
Oschlies, A. and Garcon, V.: An eddy-permitting coupled physical-biological model of the North Atlantic – 1. Sensitivity to advection numerics and mixed layer physics, Global Biogeochem. Cy., 13(1), 135–160, doi:10.1029/98GB02811, 1999.
Paulmier, A. and Ruiz-Pino, D.: Oxygen minimum zones (OMZs) in the modern ocean, Prog. Oceanogr., 80(3–4), 113–128, doi:10.1016/j.pocean.2008.08.001, 2009.
Paulmier, A., Ruiz-Pino, D., and Garcon, V.: The oxygen minimum zone (OMZ) off Chile as intense source of $CO_2$ and $N_2O$, Cont. Shelf Res., 28(20), 2746–2756, doi:10.1016/j.csr.2008.09.012, 2008.
Paulmier, A., Ruiz-Pino, D., and Garçon, V.: $CO_2$ maximum in the oxygen minimum zone (OMZ), Biogeosciences, 8, 239–252, doi:10.5194/bg-8-239-2011, 2011.
Pelegrí, J. L., Marrero-Díaz, A., and Ratsimandresey, A. W.: Nutrient irrigation of the North Atlantic, Prog. Oceanogr., 70(2–4), 366–406, doi:10.1016/j.pocean.2006.03.018, 2006.
Penven, P.: A numerical study of the southern Benguela circulation with an application to fish recruitment, Ph.D. thesis, Université de Bretagne Occidentale, Brest, France, 2000.
Penven, P., Roy, C., Brundrit, G. B., de Verdiere, A. C., Freon, P., Johnson, A. S., Lutjeharms, J. R. E., and Shillington, F. A.: A regional hydrodynamic model of upwelling in the Southern Benguela, S. Afr. J. Sci., 97(11–12), 472–475, 2001.
Penven, P., Echevin, V., Pasapera, J., Colas, F., and Tam, J.: Average circulation, seasonal cycle, and mesoscale dynamics of the Peru Current System: A modeling approach, J. Geophys. Res., 110(C10), C10021, doi:10.1029/2005JC002945, 2005.
Penven, P., Debreu, L., Marchesiello, P., and McWilliams, J. C.: Evaluation and application of the ROMS 1-way embedding procedure to the central california upwelling system, Ocean Model., 12(1–2), 157–187, doi:10.1016/j.ocemod.2005.05.002, 2006a.
Penven, P., Lutjeharms, J. R. E., and Florenchie, P.: Madagascar: A pacemaker for the Agulhas Current system?, Geophys. Res. Lett., 33, L17609, doi:10.1029/2006GL026854, 2006b.
Penven, P., Marchesiello, P., Debreu, L., and Lefèvre, J.: Software tools for pre- and post-processing of oceanic regional simulations, Environ. Modell. Softw., 23(5), 660–662, doi:10.1016/j.envsoft.2007.07.004, 2008.
Peterson, W. T., Painting, S. J., and Hutchings, L.: Diel variations in gut pigment content, diel vertical migration and estimates of grazing impact for copepods in the southern Benguela upwelling region in October 1987, J. Plankton Res., 12(2), 259–281,





BGD
8, 3537–3618, 2011



doi:10.1093/plankt/12.2.259, 1990.
Popova, E. E., Lozano, C. J., Srokosz, M. A., Fasham, M. J. R., Haley, P. J., and Robinson, A. R.: Coupled 3D physical and biological modelling of the mesoscale variability observed in North-East Atlantic in spring 1997: biological processes, Deep-Sea Res. Pt. I, 49(10), 1741–1768, doi:10.1016/S0967-0637(02)00091-2, 2002.
Quiñones, R.: An Overview of Eastern Boundary Current Systems, Chap. 2: Eastern Boundary Current Systems, in: Carbon and Nutrient Fluxes in Continental Margins: A Global Synthesis, edited by: Liu, K.-K., Atkinson, L., Quiñones, R., and Talaue-MacManus, L., Berlin, 25–29, 2010.
Ramaswamy, V., Boucher, O., Haigh, J., Hauglustaine, D., Haywood, J., Myhre, G., Nakajima, T., Shi, G., Solomon, S., Betts, R. E., Charlson, R., Chuang, C., Daniel, J. S., Del Genio, A., van Dorland, R., Feichter, J., Fuglestvedt, J., Forster, P. M., Ghan, S. J., Jones, A., Kiehl, J. T., Koch, D., Land, C., Lean, J., Lohmann, U., Minschwaner, K., Penner, J. E., Roberts, D. L., Rodhe, H., Roelofs, G. J., Rotstayn, L. D., Schneider, T. L., Schumann, U., Schwartz, S. E., Schwarzkopf, M. D., Shine, K. P., Smith, S., Stevenson, D. S., Stordal, F., Tegen, I., and Zhang, Y.: Radiative Forcing of Climate Change, in: Climate Change 2001, Working Group I: The Scientific Basis, IPCC Third Assessment Report, Cambridge University Press, New York, NY, United States(US), Pacific Northwest National Laboratory (PNNL), Richland, WA (US), 2001.
Redfield, J., Ketchum, B. H., and Richards, F. A.: The influence of organisms on the composition of sea-water, in: The sea, Vol 2, edited by: Hill, M. N., Academic Press, N.Y., 26–77, 1963.
Richardson, P. L., Lutjeharms, J. R. E., and Boebel, O.: Introduction to the "Inter-ocean exchange around southern Africa", Deep-Sea Res. Pt. II, 50(1), 1–12, doi:10.1016/S0967-0645(02)00376-4, 2003.
Robinson, C., Poulton, A. J., Holligan, P. M., Baker, A. R., Forster, G., Gist, N., Jickells, T. D., Malin, G., Upstill-Goddard, R., Williams, R. G., Woodward, E. M. S., and Zubkov, M. V.: The Atlantic Meridional Transect (AMT) Programme: A contextual view 1995–2005, Deep-Sea Res. Pt. II, 53(14–16), 1485–1515, doi:10.1016/j.dsr2.2006.05.015, 2006.
Schmid, C., Boebel, O., Zenk, W., Lutjeharms, J. R. E., Garzoli, S. L., Richardson, P. L., and Barron, C.: Early evolution of an Agulhas Ring, Deep-Sea Res. Pt. II, 50(1), 141–166, doi:10.1016/S0967-0645(02)00382-X, 2003.
Shannon, L. V., Boyd, A. J., Brundrit, G. B., and Taunton-Clark, J.: On the existence of an El Niño-type phenomenon in the Benguela System, J. Mar. Res., 44(3), 495–520,





BGD
8, 3537–3618, 2011



doi:10.1357/002224086788403105, 1986.
Shchepetkin, A. F. and McWilliams, J. C.: A method for computing horizontal pressure-gradient force in an oceanic model with a nonaligned vertical coordinate, J. Geophys. Res., 108(C3), 3090, doi:10.1029/2001JC001047, 2003.
Shchepetkin, A. F. and McWilliams, J. C.: The regional oceanic modeling system (ROMS): a split-explicit, free-surface, topography-following-coordinate oceanic model, Ocean Model., 9(4), 347–404, doi:10.1016/j.ocemod.2004.08.002, 2005.
Siegfried, W. R., Crawford, R. J. M., Shannon, L. V., Pollock, D. E., Payne, A. I. L., and Krohn, R. G.: Scenarios for global-warming induced change in the open-ocean environment and selected fisheries of the west coast of Southern Africa, S. Afr. J. Sci., 86(7–10), 281–285, 1990.
Silio-Calzada, A., Bricaud, A., Uitz, J., and Gentili, B.: Estimation of new primary production in the Benguela upwelling area, using ENVISAT satellite data and a model dependent on the phytoplankton community size structure, J. Geophys. Res., 113, C11023, doi:10.1029/2007JC004588, 2008.
Stramma, L., Johnson, G. C., Sprintall, J., and Mohrholz, V.: Expanding oxygen-minimum zones in the tropical oceans, Science, 320(5876), 655–658, doi:10.1126/science.1153847, 2008.
Stramma, L., Johnson, G. C., Firing, E., and Schmidtko, S.: Eastern Pacific oxygen minimum zones: Supply paths and multidecadal changes, J. Geophys. Res., 115, C09011, doi:201010.1029/2009JC005976, 2010.
Taylor, K. E.: Summarizing multiple aspects of model performance in a single diagram, J. Geophys. Res., 106(D7), 7183–7192, 2001.
Tian, R. C., Vézina, A., Legendre, L., Ingram, R. G., Klein, B., Packard, T., Roy, S., Savenkoff, C., Silverberg, N., Therriault, J. C., and Tremblay, J. E.: Effects of pelagic food-web interactions and nutrient remineralization on the biogeochemical cycling of carbon: a modeling approach, Deep-Sea Res. Pt. II, 47(3–4), 637–662, doi:10.1016/S0967-0645(99)00121-6, 2000.
Tian, R. C., Vézina, A. F., Starr, M., and Saucier, F.: Seasonal dynamics of coastal ecosystems and export production at high latitudes: A modeling study, Limnol. Oceanogr., 46(8), 1845–1859, doi:10.4319/lo.2001.46.8.1845, 2001.
Tilstone, G., Smyth, T., Poulton, A., and Hutson, R.: Measured and remotely sensed estimates of primary production in the Atlantic Ocean from 1998 to 2005, Deep-Sea Res. Pt. II, 56(15),





BGD
8, 3537–3618, 2011



918–930, doi:10.1016/j.dsr2.2008.10.034, 2009.
Tyrrell, T. and Lucas, M. I.: Geochemical evidence of denitrification in the Benguela upwelling system, Cont. Shelf Res., 22(17), 2497–2511, 2002.
Veitch, J., Penven, P., and Shillington, F.: The Benguela: A laboratory for comparative modeling studies, Prog. Oceanogr., 83(1–4), 296–302, doi:10.1016/j.pocean.2009.07.008, 2009.
Verheye, H. M. and Ekau, W.: Geochemistry and Ecology of the Namibian Upwelling System (GENUS Project) and St Helena Bay Monitoring Line (SHBML), cruise report, FRS Africana, 1–17 December 2009.
Wanninkhof, R.: Relationship Between Wind Speed and Gas Exchange Over the Ocean, J. Geophys. Res., 97, 7373–7382, 1992.
Walter, S., Bange, H. W., Breitenbach, U., and Wallace, D. W. R.: Nitrous oxide in the North Atlantic Ocean, Biogeosciences, 3, 607–619, doi:10.5194/bg-3-607-2006, 2006.
Ware, D. M.: Production characteristics of upwelling systems and the trophodynamic roleof hake, in: Benguela trophic functioning, edited by: Payne, A. I. L., Brink, K. H., Mann, K. H., and Hilborn, R., 501–513, 1992.
Weiss, R. F. and Price, B. A.: Nitrous oxide solubility in water and seawater, Mar. Chem., 8(4), 347–359, doi:10.1016/0304-4203(80)90024-9, 1980.
Wittke, F., Kock, A., and Bange, H. W.: Nitrous oxide emissions from the upwelling area off Mauritania (NW Africa), Geophys. Res. Lett., 37, L12601, doi:201010.1029/2010GL042442, 2010.
Yakushev, E. V., Pollehne, F., Jost, G., Kuznetso, I., Schneider, B., and Urnlauf, L.: Analysis of the water column oxic/anoxic interface in the Black and Baltic seas with a numerical model, Mar. Chem., 107(3), 388–410, doi:10.1016/j.marchem.2007.06.003, 2007.
Zabel, M. and cruise participants: Report and preliminary results of METEOR Cruise M57/2, Walvis Bay–Walvis Bay, 11.02.–12.03.2003, cruise report, Berichte, Fachbereich Geowissenschaften, Universität Bremen, 220, 2003.





BGD
8, 3537–3618, 2011



**Table 1.** BioBUS biogeochemical model state variables (symbols and units), initial surface values used for the simulation, and scale depth considered for the exponential decrease with depth (for $P_S$, $P_L$, $NO_2$, $NH_4$, $Z_S$, $Z_L$ and DON).

| Symbol | Variable | Unity | Initial values | Scale depth (m) |
|---|---|---|---|---|
| $P_S$ | Nanophytoplankton (flagellates) | mmol N $m^{-3}$ | 0.04[a] | 50 |
| $P_L$ | Microphytoplankton (diatoms) | mmol N $m^{-3}$ | 0.06[a] | 50 |
| $NO_3$ | Nitrates | mmol N $m^{-3}$ | CARS[b] | – |
| $NO_2$ | Nitrites | mmol N $m^{-3}$ | 0.05 | 100 |
| $NH_4$ | Ammonium | mmol N $m^{-3}$ | 0.1[a] | 100 |
| $Z_S$ | Microzooplankton (ciliates) | mmol N $m^{-3}$ | 0.04[a] | 100 |
| $Z_L$ | Mesozooplankton (copepods) | mmol N $m^{-3}$ | 0.04[a] | 100 |
| $D_S$ | Small detritus | mmol N $m^{-3}$ | 0.02[a] | constant with depth |
| $D_L$ | Large detritus | mmol N $m^{-3}$ | 0.02[a] | constant with depth |
| DON | Dissolved Organic Nitrogen | mmol N $m^{-3}$ | 0.5 | 100 |
| $O_2$ | Dissolved Oxygen | mmol $O_2$ $m^{-3}$ | CARS[b] | – |
| $N_2O$ | Nitrous oxide | mmol $N_2O$ $m^{-3}$ | $f([O_2])$[c] | – |

[a] Koné et al. (2005).
[b] CARS database (2006).
[c] (Nevison et al., 2003) parameterization: $[N_2O]$ is a function of $[O_2]$.





BGD
8, 3537–3618, 2011



**Table 2.** BioBUS biogeochemical model parameter values. We remind the references used by Koné et al. (2005) in their modeling study.

| Parameter | Symbol | Units | Value | References |
|---|---|---|---|---|
| Phytoplankton | | | | |
| Initial slope of P-I curve for $P_S$ | $\alpha_{P_S}$ | $m^2\,W^{-1}\,d^{-1}$ | 0.025 | OG99, K05 |
| Initial slope of P-I curve for $P_L$ | $\alpha_{P_L}$ | $m^2\,W^{-1}\,d^{-1}$ | 0.04 | Popova et al. (2002), K05 |
| Light attenuation coefficient due to pure water | $k_w$ | $m^{-1}$ | 0.04 | OG99, T00, K05 |
| Light attenuation coefficient by phytoplankton | $k_{chl\text{-}a}$ | $m^2\,mg\,Chl^{-1}$ | 0.024 | OC00, K05 |
| Chl/C ratio | $\theta$ | $mg\,Chl\,mg\,C^{-1}$ | 0.02 | F90, Lacroix and Nival (1998), T00, K05 |
| Maximum growth rate for $P_S$ | $a_{P_S}$ | $d^{-1}$ | 0.557 | K05 |
| Maximum growth rate for $P_L$ | $a_{P_L}$ | $d^{-1}$ | 0.6 | Adjusted |
| | $b$ | – | 1.066 | OG99, K05 |
| | $c$ | $(°C)^{-1}$ | 1 | OG99, K05 |
| Mortality rate of $P_S$ | $\mu_{P_S}$ | $d^{-1}$ | 0.027 | K05 |
| Mortality rate of $P_L$ | $\mu_{P_L}$ | $d^{-1}$ | 0.03 | OG99, K05 |
| Exudation fraction of primary production (by $P_S$) | $\varepsilon_{P_S}$ | $d^{-1}$ | 0.05 | H05, Y07 |
| Exudation fraction of primary production (by $P_L$) | $\varepsilon_{P_L}$ | $d^{-1}$ | 0.05 | H05, Y07 |
| Strength of $NH_4$ inhibition of $NO_3$ uptake constant | $K_{psi}$ | $(mmol\,N\,m^{-3})^{-1}$ | 1.46 | Y07 |
| Half saturation constant for uptake of $NH_4$ by $P_S$ | $K_{NH_{4P_S}}$ | $mmol\,N\,m^{-3}$ | 0.5 | K05 |
| Half saturation constant for uptake of $NH_4$ by $P_L$ | $K_{NH_{4P_L}}$ | $mmol\,N\,m^{-3}$ | 1 | Adjusted |
| Half saturation constant for uptake of $NO_3 + NO_2$ by $P_S$ | $K_{NO_{3P_S}}$ | $mmol\,N\,m^{-3}$ | 0.5 | Adjusted |
| Half saturation constant for uptake of $NO_3 + NO_2$ by $P_L$ | $K_{NO_{3P_L}}$ | $mmol\,N\,m^{-3}$ | 2 | K05 |
| C/N ratio for phytoplankton | $R_{C/N}$ | $mol\,C\,mol\,N^{-1}$ | 106/16 | Redfield et al. (1963) |
| $O_2$/N ratio | $R_{O_2/N}$ | $mol\,O_2\,mol\,N^{-1}$ | 170/16 | Conkright and O'Brien (1994) |
| Sedimentation velocity of $P_L$ | $w_{P_L}$ | $m\,d^{-1}$ | 0.5 | K05 |
| Zooplankton | | | | |
| Assimilation efficiency of $Z_S$ | $f1_{Z_S}$ | – | 0.75 | K05 |
| Assimilation efficiency of $Z_L$ | $f1_{Z_L}$ | – | 0.7 | K05 |
| Maximum grazing rate of $Z_S$ | $g_{max_{Z_S}}$ | $d^{-1}$ | 0.9 | Adjusted |
| Maximum grazing rate of $Z_L$ | $g_{max_{Z_L}}$ | $d^{-1}$ | 1.2 | Adjusted |
| Preference of $Z_S$ for $P_S$ | $e_{Z_SP_S}$ | – | 0.7 | Adjusted |
| Preference of $Z_S$ for $P_L$ | $e_{Z_SP_L}$ | – | 0.3 | Adjusted |





BGD
8, 3537–3618, 2011



**Table 2.** Continued.

| Parameter | Symbol | Units | Value | References |
|---|---|---|---|---|
| Zooplankton | | | | |
| Preference of $Z_L$ for $P_S$ | $e_{Z_L P_S}$ | – | 0.26 | Adjusted |
| Preference of $Z_L$ for $P_L$ | $e_{Z_L P_L}$ | – | 0.53 | Adjusted |
| Preference of $Z_L$ for $Z_S$ | $e_{Z_L Z_S}$ | – | 0.21 | Adjusted |
| Half saturation constant for ingestion by $Z_S$ | $k_{Z_S}$ | mmol N $m^{-3}$ | 1.5 | Adjusted |
| Half saturation constant for ingestion by $Z_L$ | $k_{Z_L}$ | mmol N $m^{-3}$ | 4 | Adjusted |
| Mortality rate of $Z_S$ | $\mu_{Z_S}$ | (mmol N $m^{-3}$)$^{-1}$ $d^{-1}$ | 0.025 | K05 |
| Mortality rate of $Z_L$ | $\mu_{Z_L}$ | (mmol N $m^{-3}$)$^{-1}$ $d^{-1}$ | 0.05 | OC00, K05 |
| Excretion rate of $Z_S$ | $\gamma_{Z_S}$ | $d^{-1}$ | 0.05 | Adjusted |
| Excretion rate of $Z_L$ | $\gamma_{Z_L}$ | $d^{-1}$ | 0.05 | K05 |
| Organic fraction of $Z_S$ excretion | $f2_{Z_S}$ | – | 0.25 | F90 |
| Organic fraction of $Z_L$ excretion | $f2_{Z_L}$ | – | 0.25 | F90 |
| Detritus | | | | |
| Hydrolysis rate of $D_S$ | $\mu_{D_S}$ | $d^{-1}$ | 0.12 | Adjusted |
| Hydrolysis rate of $D_L$ | $\mu_{D_L}$ | $d^{-1}$ | 0.08 | Adjusted |
| Sedimentation velocity of $D_S$ | $w_{D_S}$ | m $d^{-1}$ | 1 | K05 |
| Sedimentation velocity of $D_L$ | $w_{D_L}$ | m $d^{-1}$ | 20 | Adjusted |
| Mineralisation in oxic conditions | | | | |
| Mineralisation rate of DON | $K_{ND4}$ | $d^{-1}$ | 0.002 | Adjusted |
| Mineralisation rate of PON | $K_{NP4}$ | $d^{-1}$ | 0.007 | Adjusted |
| Temperature parameter | $K$tox | $(°C)^{-1}$ | 0,15 | Y07 |
| Oxygen parameter | $O_2$ox | mmol $O_2$ $m^{-3}$ | 0 | Y07 |
| Half saturation constant | $K$ox | mmol $O_2$ $m^{-3}$ | 15 | Y07 |





BGD
8, 3537–3618, 2011



**Table 2.** Continued.

| Parameter | Symbol | Units | Value | References |
|---|---|---|---|---|
| Denitrification | | | | |
| Rate of 1st stage of denitrification | $K_{N32}$ | $d^{-1}$ | 0.12 | Y07 |
| Rate of 2nd stage of denitrification | $K_{N24}$ | $d^{-1}$ | 0.2 | Y07 |
| Oxygen parameter | $O_2$dn | mmol $O_2$ $m^{-3}$ | 25 | Y07 |
| $NO_3$ parameter | $NO_3$mi | mmol N $m^{-3}$ | 0.001 | Y07 |
| $NO_2$ parameter | $NO_2$mi | mmol N $m^{-3}$ | 0.0001 | Y07 |
| Nitrification | | | | |
| Rate of 1st stage of Nitrification | $K_{N42}$ | $d^{-1}$ | 0.9 | Y07 |
| Rate of 2nd stage of Nitrification | $K_{N23}$ | $d^{-1}$ | 2.5 | Y07 |
| $O_2$ parameter | $O_2$nf | mmol $O_2$ $m^{-3}$ | 1 | Y07 |
| Anammox | | | | |
| Anammox constant | $K_{anammox}$ | $d^{-1}$ | 0.03 | Y07 |
| Conversion constant | $K_{convert}$ | (mmol N $m^{-3}$)$^{-1}$ | 1 | Yakushev, personal communication (2009) |
| $N_2O$ formulation | | | | |
| N/$O_2$ ratio | $R_{N/O_2}$ | mol N mol $O_2^{-1}$ | 16/170 | Conkright and O'Brien (1994) |
| | $a_1$ | mol $N_2O$ mol $N^{-1}$ (mmol $O_2$ $m^{-3}$)$^{-1}$ | 0.26 | N03 |
| | $a_2$ | mol $N_2O$ mol $N^{-1}$ | −0.0004 | N03 |
| depth scale | $Z_{scale}$ | m | 3000 | N03 |

OG99: Oschlies and Garcon (1999); K05: Koné et al. (2005); OC00: Olivieri and Chavez (2000); T00: Tian et al. (2000); H05: Huret et al. (2005); Y07: Yakushev et al. (2007); F90: Fasham et al. (1990); N03: Nevison et al. (2003).





BGD
8, 3537–3618, 2011



**Table 3.** Parameter values for the sensitivity analyses (the final values are indicated in bold). Reference stands for the reference run (explained in the text) and Ref/10, Ref/5, Ref/2, Ref × 2, Ref × 5, Ref × 10 for the value of the reference run divided by a factor of 10, 5 and 2, multiplied by a factor of 2, 5 and 10, respectively.

| Parameter | Symbol | Units | Ref | Ref/10 | Ref/5 | Ref/2 | Ref × 2 | Ref × 5 | Ref × 10 |
|---|---|---|---|---|---|---|---|---|---|
| Phytoplankton | | | | | | | | | |
| Half saturation constant for uptake of $NO_3$+$NO_2$ by $P_S$ | $K_{NO_{3P_S}}$ | mmol N $m^{-3}$ | **0.5** | | | | 1 | 2.5 | |
| Zooplankton | | | | | | | | | |
| Excretion rate of $Z_S$ | $\gamma_{Z_S}$ | $d^{-1}$ | **0.05** | 0.005 | | | | | |
| Detritus | | | | | | | | | |
| Sedimentation velocity of $D_L$ | $w_{D_L}$ | m $d^{-1}$ | 10 | | | | **20** | 50 | 100 |
| Mineralisation in oxic conditions | | | | | | | | | |
| Mineralisation rate of DON | $K_{ND4}$ | $d^{-1}$ | 0.02 | **0.002** | | 0.01 | 0.04 | 0.1 | |
| Mineralisation rate of PON ($D_L$) | $K_{NP4}$ | $d^{-1}$ | **0.007** | | 0.0014 | 0.0035 | 0.014 | | |





BGD
8, 3537–3618, 2011



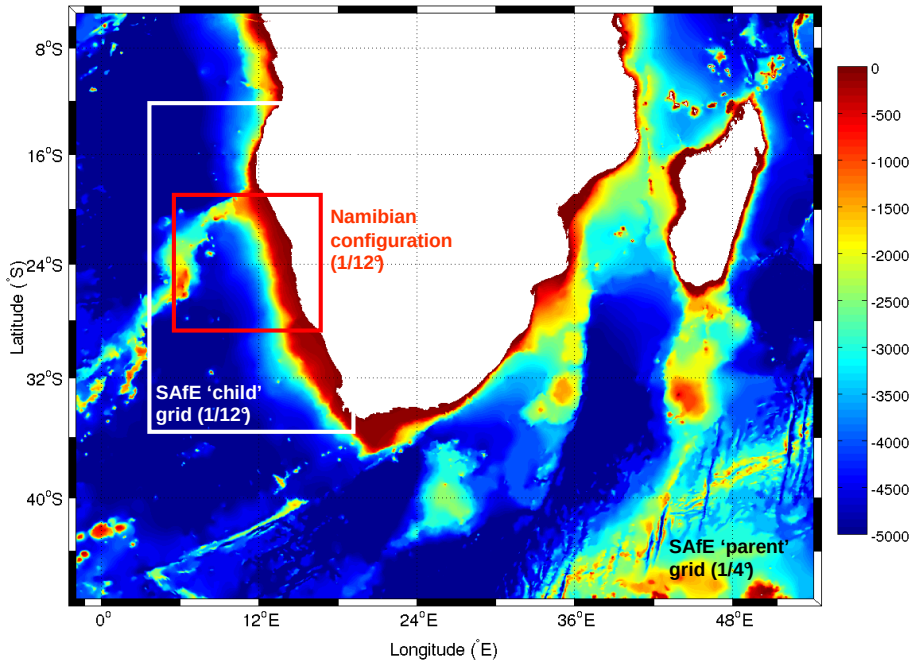


**Fig. 1.** Bathymetry (in meters) from 1′ GEBCO. Domain of the Southern Africa Experiment (SAfE "parent" grid; 2.5° W–54.75° E and 4.8° S–46.75° S, 1/4°). The high resolution domain (SAfE "child" grid; 3.9° E–19.8° E and 12.1° S–35.6° S, 1/12°) is represented by the domain within the white rectangle, and the Namibian configuration (5° E–17° E and 19° S–28.5° S, 1/12°) developed and validated in this study depicts the domain within the red rectangle.





BGD
8, 3537–3618, 2011



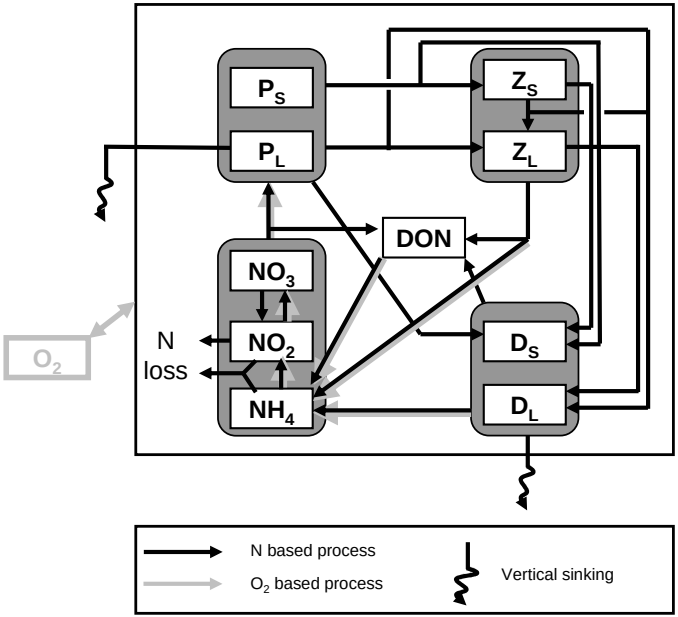


**Fig. 2.** Interactions between the different compartments of the BioBUS biogeochemical model. Black arrows represent the nitrogen-dependent processes, and arrows with added gray colors the oxygen-dependent processes. Arrows from or to a gray rectangle act on all variables included in this gray rectangle.





BGD
8, 3537–3618, 2011



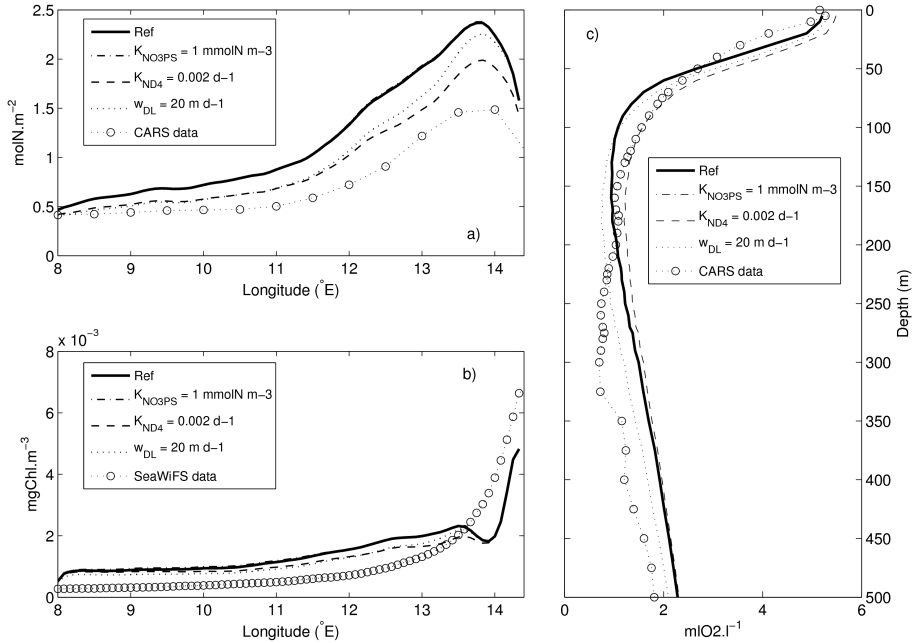


**Fig. 3.** Sensitivity analyses for the parameters $K_{NO_{3PS}}$ (small phytoplankton nitrate uptake; dotted-dashed line), $K_{ND4}$ (DON mineralization rate; dashed line) and $w_{D_L}$ (large detritus sedimentation velocity; dotted line) compared to the reference values (solid line) for these parameters and the climatology (dotted line with circles) (see Table 3 and the text for explanation). **(a)** Annual mean of 0–100 m integrated nitrate concentrations (mmol N $m^{-2}$) along an east-west profile (averaged between 22° S–24° S), **(b)** annual mean of Chl-*a* (mg Chl $m^{-3}$) using a Chl/N ratio equal to 1 g Chl (mol N)$^{-1}$ along the same east-west profile, and **(c)** vertical profile of annual mean oxygen concentrations (ml $O_2$ $l^{-1}$) (averaged between 22° S–24° S and 13° E–15° E). The sensitivity analysis for the parameter $K_{NO_{3PS}}$ gives the same result as the reference (the dashed-dotted line is masked by the solid line).





BGD
8, 3537–3618, 2011



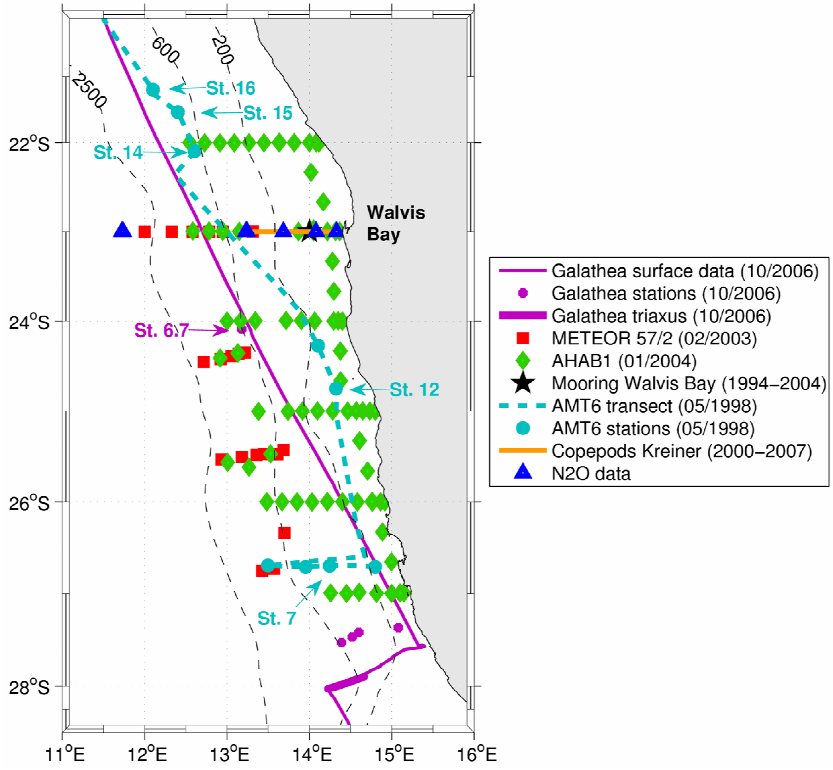


**Fig. 4.** Cruise sections and stations used for the model/data comparison: the Danish Galathea expedition (October 2006), the METEOR expedition 57/2 (February 2003), the AHAB1 expedition (January 2004), AMT 6 cruise (May 1998), the Walvis Bay mooring at 23° S between 1994 and 2004 (Monteiro and van der Plas, 2006), and the time series of copepod abundance from the coast (14.5° E) to 70 nautical miles (13.23° E) off Walvis Bay at 23° S between 2000 to 2007 (Kreiner and Ayon, 2008). The black dashed lines indicate the bathymetry (in meters). Specific stations are indicated and will be discussed later in the text.





BGD
8, 3537–3618, 2011



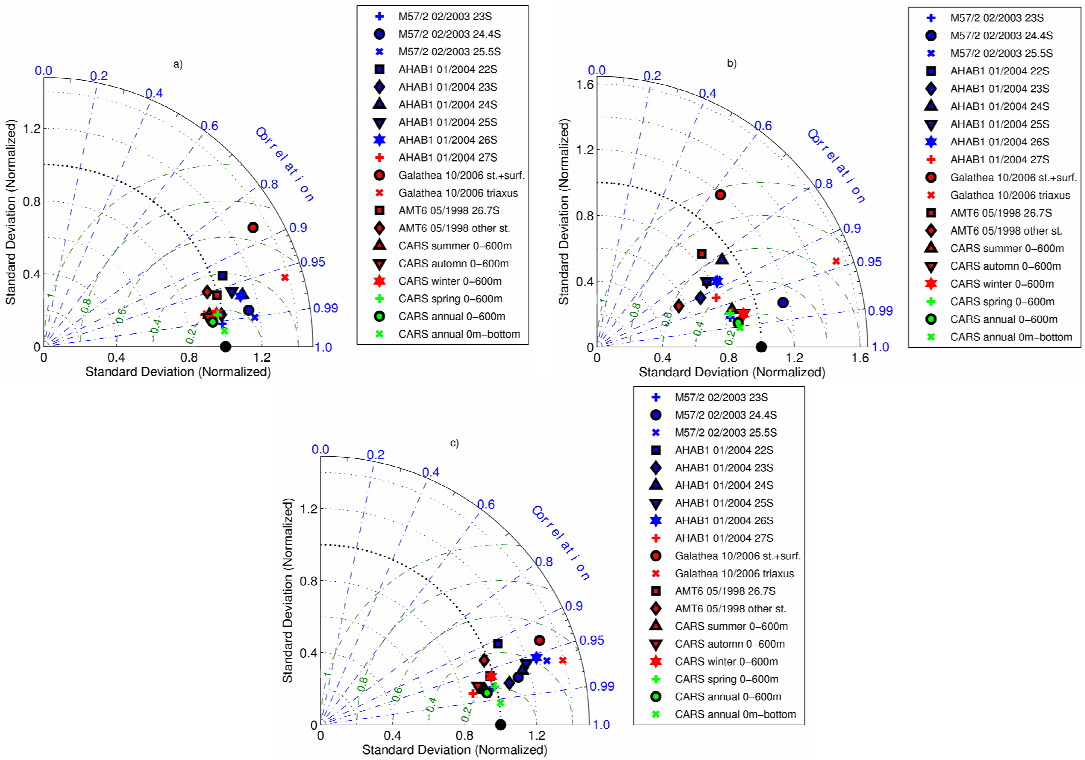


**Fig. 5.** Taylor's diagrams for **(a)** Temperature, **(b)** Salinity, and **(c)** Density. The radial distance from the origin is proportional to the standard deviation of a pattern (normalized by the data standard deviation). The green dashed lines measure the distance from the reference point (data) and indicate the RMS error (see the expression in Sect. 4). The correlation between both fields is given by the azimuthal position of the test field. The statistics use data from the METEOR expedition 57/2 in February 2003 (transects at 23° S, 24.4° S, and 25.5° S), the AHAB1 expedition in January 2004 (transects at 22° S, 23° S, 24° S, 25° S, 26° S, and 27° S), the Galathea data in October 2006 (surface data, 5 stations, and triaxus data), the AMT 6 cruise in May 1998 (transect at 26.7° S and 4 stations), and the CARS database (2009) (seasonal and annual mean). For the comparison with in-situ data, simulated fields were monthly averaged (note there are 10 outputs by month) using the last year of simulation (year 12). For the comparison with CARS database, simulated fields were either seasonally or annually averaged. The reference is indicated by the black filled circle.





BGD
8, 3537–3618, 2011

Nitrogen transfers and air-sea $N_2O$ fluxes in the upwelling off Namibia

E. Gutknecht et al.



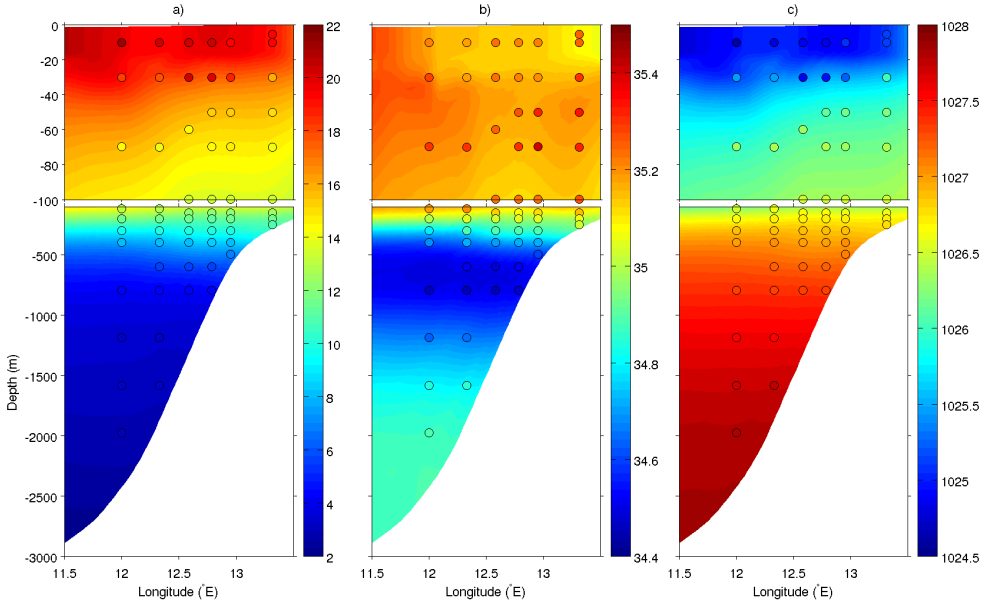


**Fig. 6. (a)** Temperature (°C), **(b)** salinity, **(c)** density (kg m$^{-3}$) estimated with the coupled model at 23° S. Simulated fields represent the mean situation for the climatological month of February. Colored circles overlaid on the simulated fields (using the same color bar) correspond to the METEOR 57/2 data, in February 2003.





BGD
8, 3537–3618, 2011



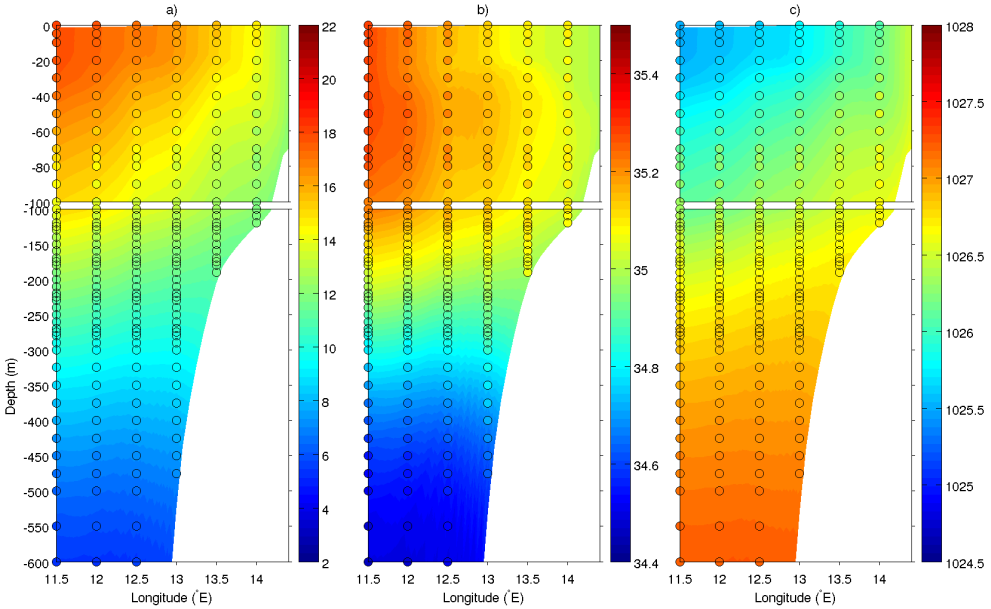


**Fig. 7.** Simulated annual mean of **(a)** temperature (°C), **(b)** salinity, and **(c)** density ($kg\,m^{-3}$) at 23° S between the surface and 600-m depth. Colored circles for the annual mean CARS database (2009) are overlaid on the simulated fields using the same color bar as the simulated fields.





BGD
8, 3537–3618, 2011



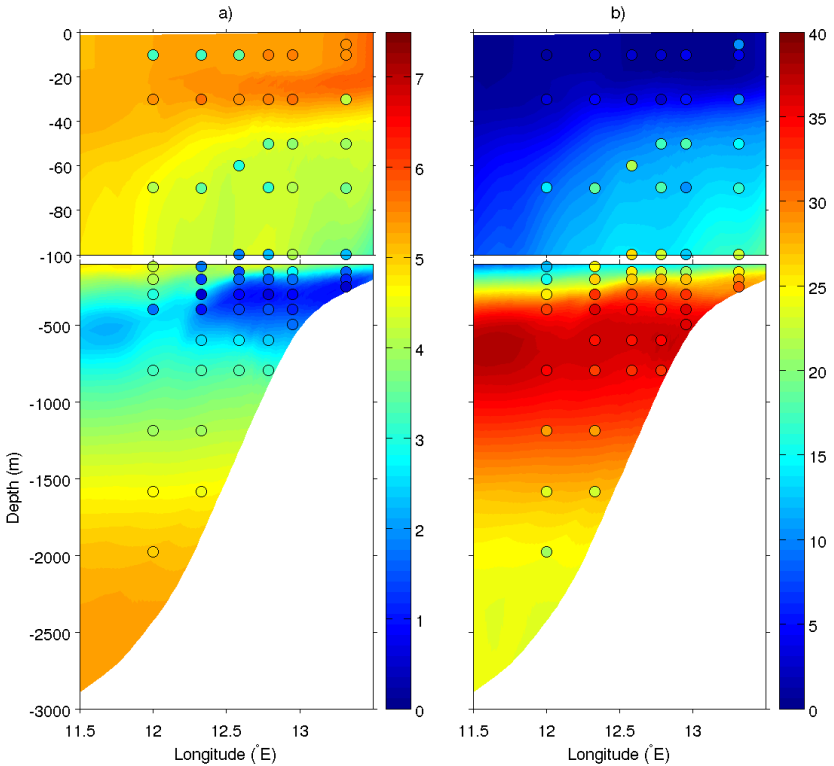


**Fig. 8.** **(a)** Oxygen ($ml\,O_2\,l^{-1}$) and **(b)** nitrate ($mmol\,N\,m^{-3}$) concentrations estimated with the coupled model at 23° S. Simulated fields represent the mean situation for the climatological month of February. Colored circles overlaid on the simulated fields (using the same color bar) correspond to the METEOR 57/2 data, in February 2003.





BGD
8, 3537–3618, 2011



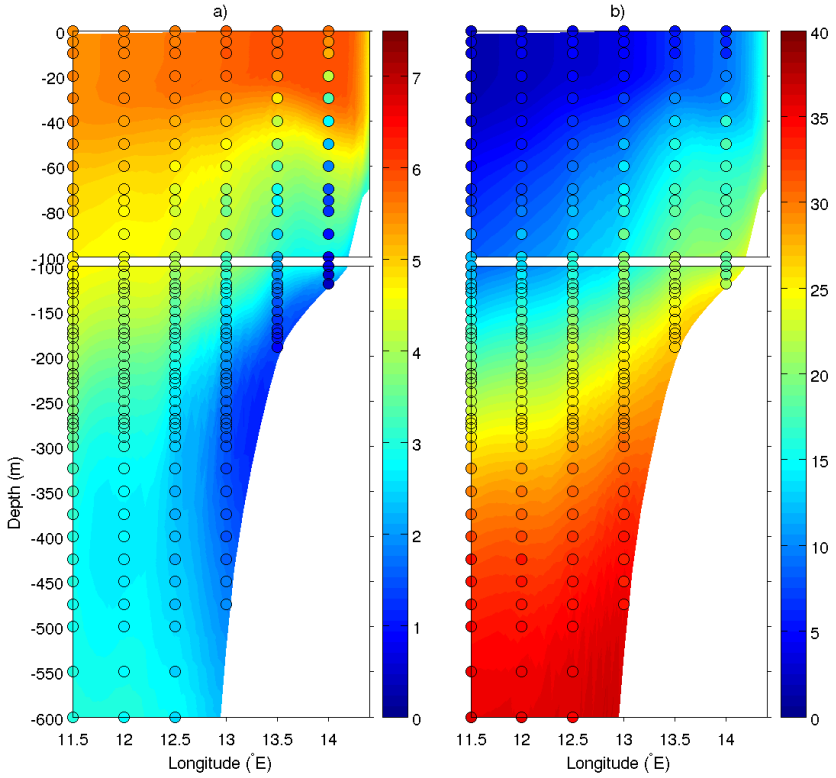


**Fig. 9.** Simulated annual mean of **(a)** oxygen (ml $O_2$ $l^{-1}$) and **(b)** nitrate (mmol N $m^{-3}$) concentrations at 23° S and between 0 and 600 m. Colored circles for the annual mean of CARS database (2009) are overlaid on the simulated fields using the same color bar as the simulated fields.





BGD
8, 3537–3618, 2011



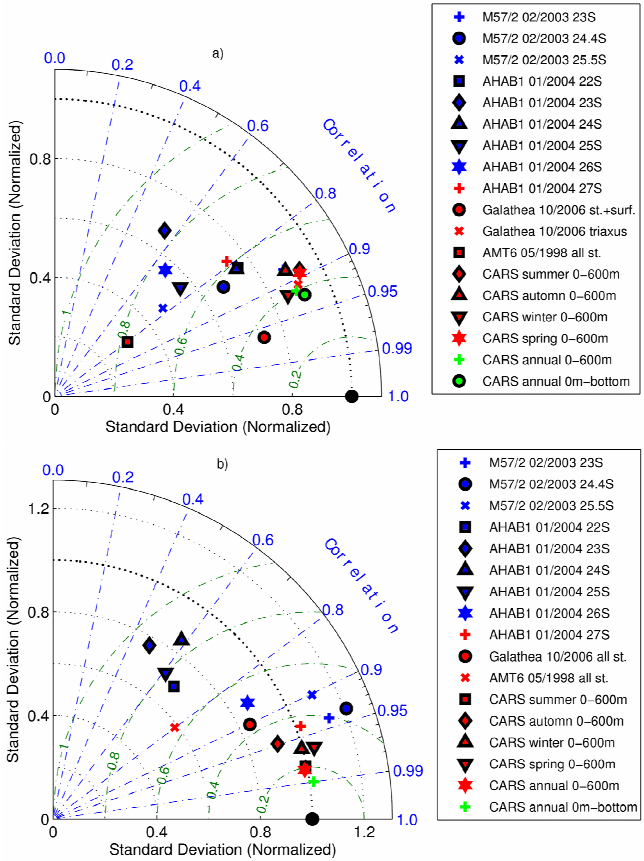


**Fig. 10.** Taylor's diagrams for **(a)** oxygen and **(b)** nitrate concentrations. See legend of Fig. 5 for details and abbreviations.





BGD
8, 3537–3618, 2011



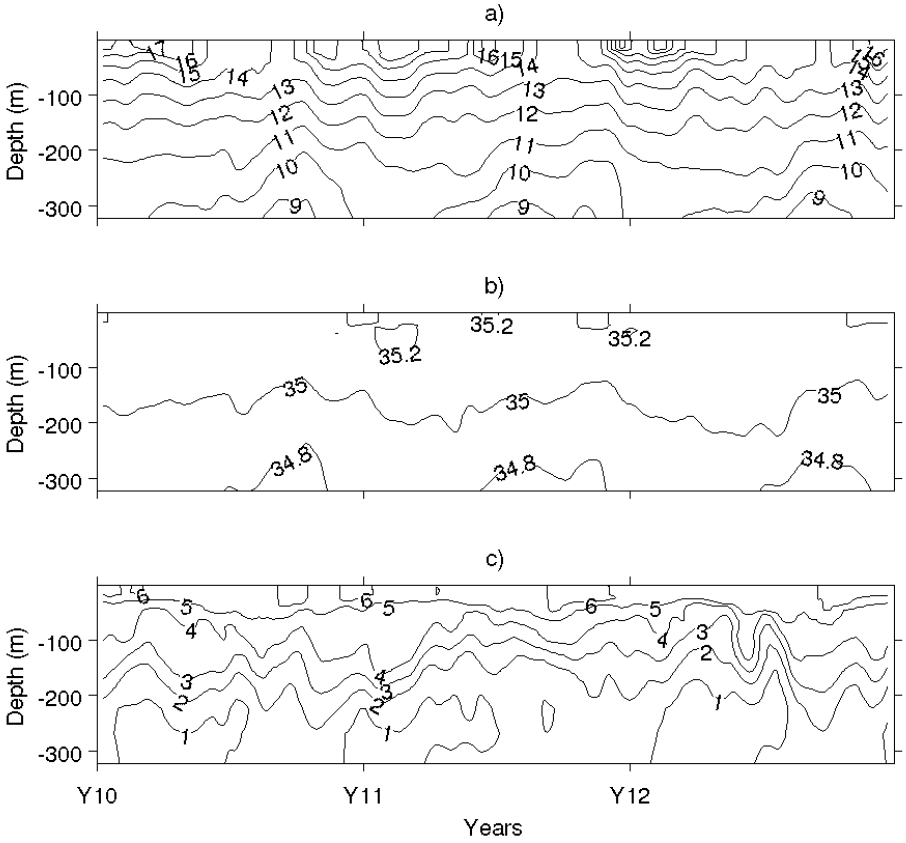


**Fig. 11.** Temporal evolution (last 3 yr of simulation) of the vertical profiles of **(a)** temperature (°C), **(b)** salinity, and **(c)** oxygen (ml $O_2$ $l^{-1}$) at 23° S–14° E (Walvis Bay mooring).





BGD
8, 3537–3618, 2011



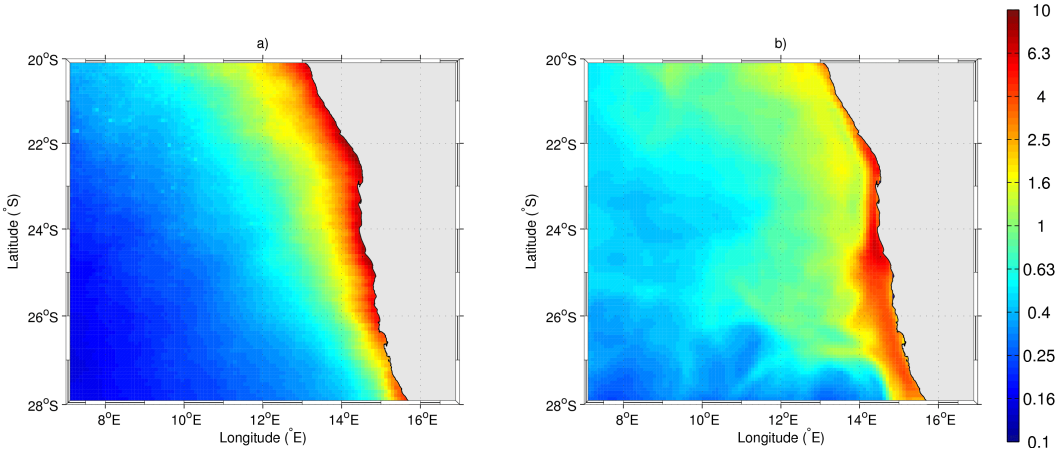


**Fig. 12.** Annual mean of Chl-*a* (mg Chl $m^{-3}$) from **(a)** SeaWiFS sensor and **(b)** the coupled model.





BGD
8, 3537–3618, 2011



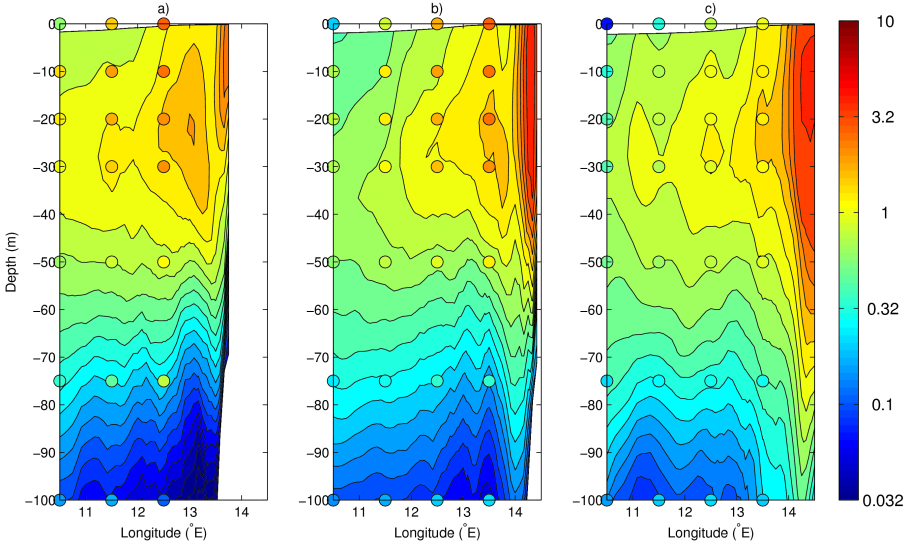


**Fig. 13.** Annual mean of simulated Chl-*a* (mg Chl $m^{-3}$) at **(a)** 21.5° S, **(b)** 23.5° S, and **(c)** 25.5° S. Chl-*a* from Annual WOA climatology (2001; Conkright et al., 2002) are overlaid using the same color bar as the simulated fields.





BGD
8, 3537–3618, 2011



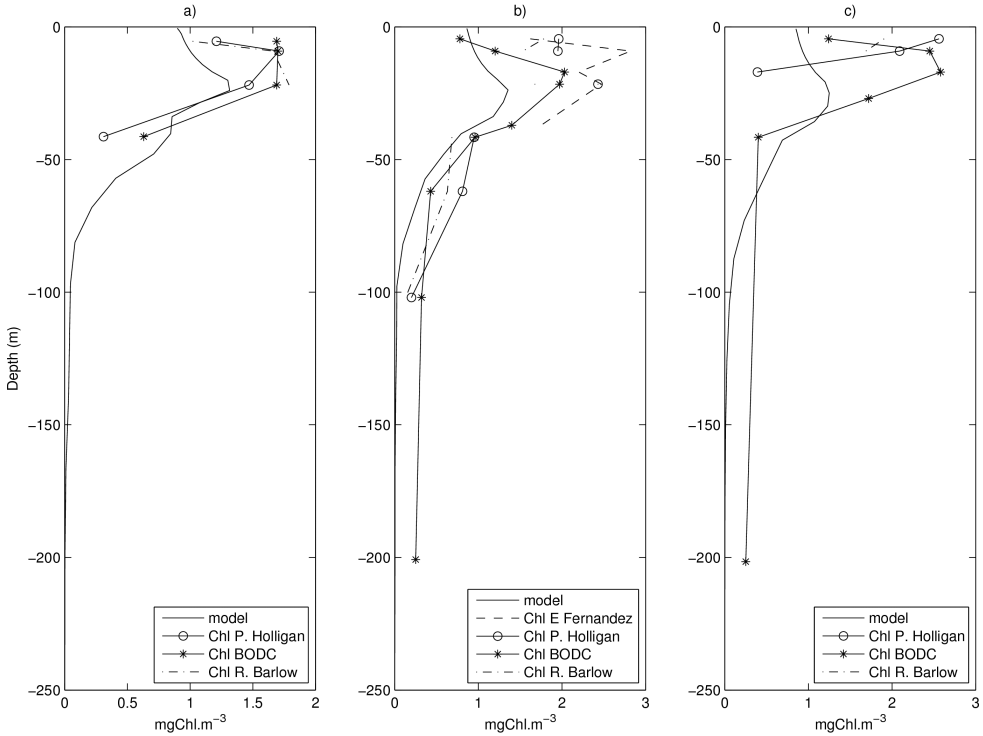


**Fig. 14.** Vertical profiles of Chl-*a* (mg Chl m$^{-3}$) at stations 14 **(a)**, 15 **(b)**, and 16 **(c)**. The black solid line represents the simulated field (averaged climatological month of May). The other black lines represent the estimations made during the AMT 6 cruise, in May 1998, from four different sources (E. Fernandez for the dashed line, P. Holligan for the circles, the British Oceanographic Data Center for the stars, and R. Barlow for the dashed-dotted line).





BGD
8, 3537–3618, 2011



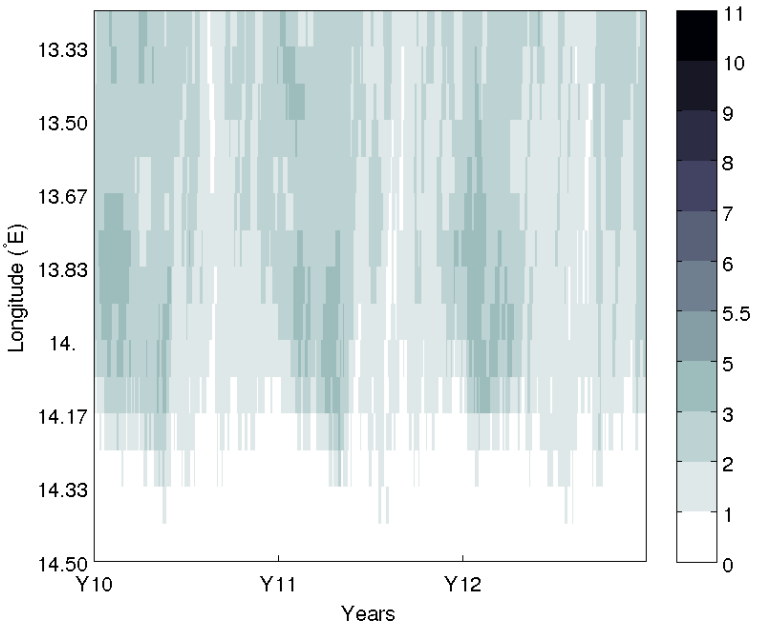


**Fig. 15.** Copepod abundance ($10^5$ no m$^{-2}$) integrated over the first 200 m at 23° S, for the last 3 yr of the simulation.





BGD
8, 3537–3618, 2011



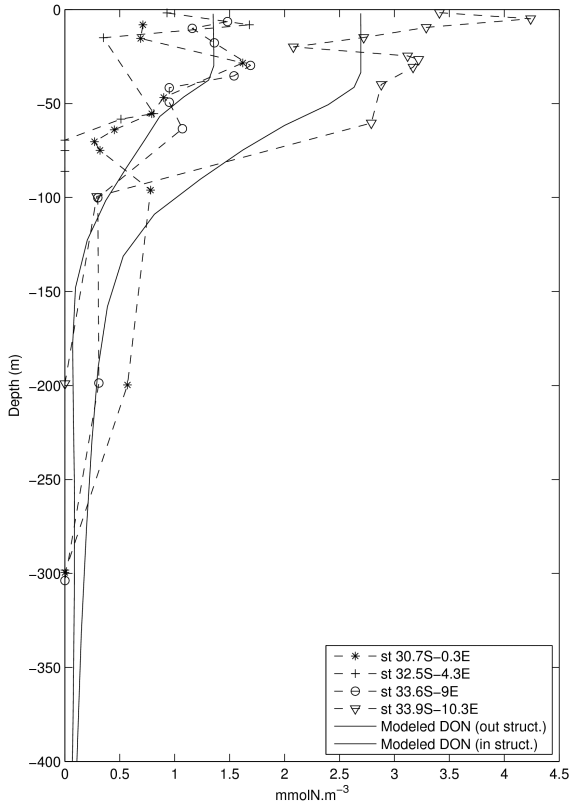


**Fig. 16.** Semi-labile DON concentrations (mmol N $m^{-3}$) estimated at four stations in the open ocean during the AMT 17 cruise (profiles with dashed lines), in November 2005, and estimated from the coupled model (solid lines), for an averaged climatological month of November. Simulated vertical profiles were taken in the open ocean, one in a physical structure (filament; in struct. on the plot) and the other outside of this structure (out struct. on the plot).





BGD
8, 3537–3618, 2011



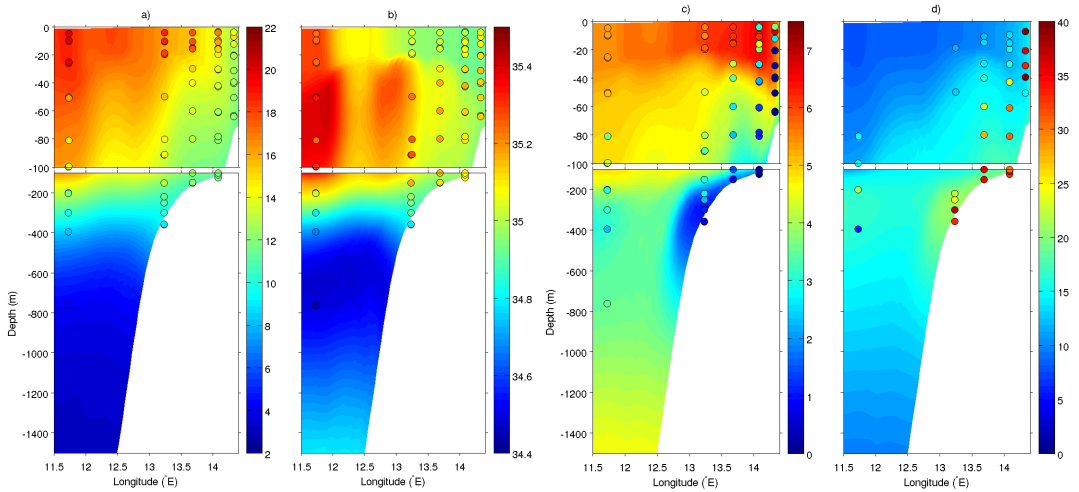


**Fig. 17.** **(a)** Temperature (°C), **(b)** salinity, **(c)** oxygen (ml $O_2$ $l^{-1}$), and **(d)** nitrous oxide (nmol $N_2O$ $l^{-1}$) concentrations estimated with the coupled model at 23° S. Colored circles for the FRS Africana (December 2009) data are overlaid on the modeled fields using the same color bar as the modeled fields.





BGD
8, 3537–3618, 2011



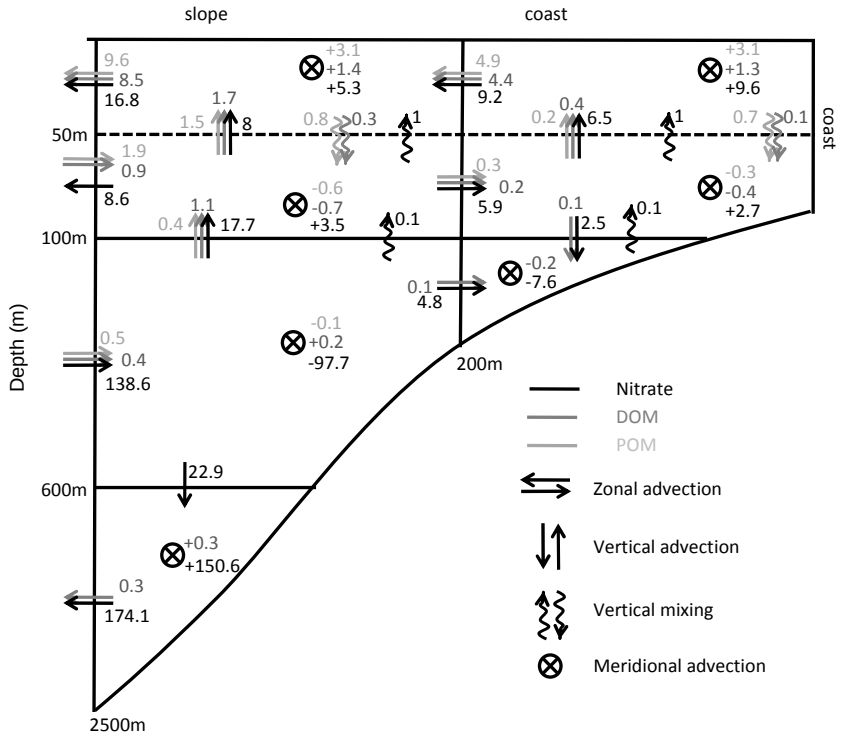


**Fig. 18.** Annual nitrogen budget performed around Walvis Bay (between 22° S and 24° S) for physical fluxes for nitrates (black arrow), DOM (dark gray), and POM (light gray). Integrated fluxes are in $10^{10}$ mol N yr$^{-1}$. Fluxes lower than $10^{7}$ mol N yr$^{-1}$ are not reported on the figure. Horizontal (vertical) arrows represent the zonal (vertical) advection, wavy arrows the vertical mixing, and cross-circles the meridional advection.





BGD
8, 3537–3618, 2011



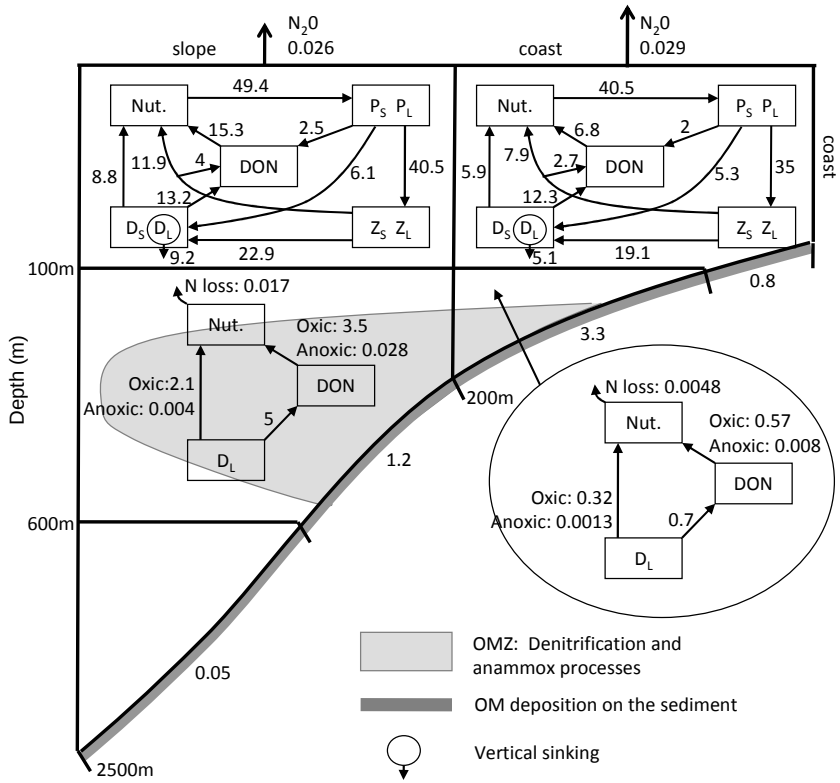


**Fig. 19.** Annual nitrogen budget performed around Walvis Bay (between 22° S and 24° S) for biogeochemical fluxes of the BioBUS model. Integrated fluxes are in $10^{10}$ mol N yr$^{-1}$. Fluxes lower than $10^{7}$ mol N yr$^{-1}$ are not reported on the figure. The different compartments of BioBUS were summarized to highlight the dominant processes in each sub-domain.





BGD
8, 3537–3618, 2011



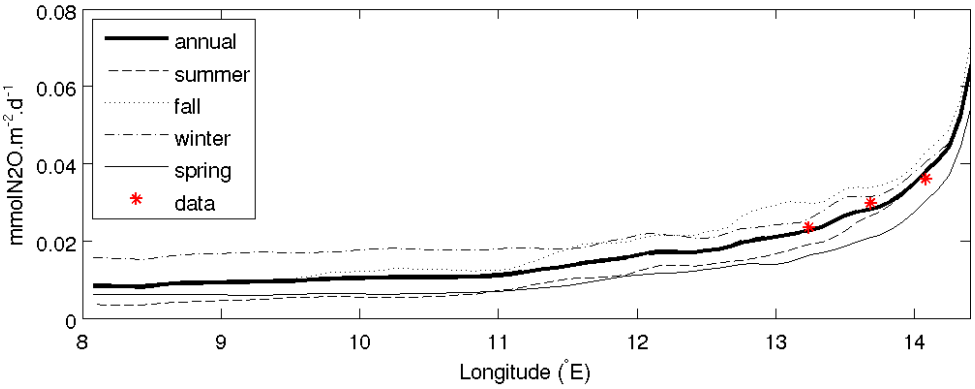


**Fig. 20.** Annual and seasonal mean of air-sea $N_2O$ fluxes (mmol $N_2O$ $m^{-2}$ $d^{-1}$), averaged over the latitude range 22° S to 24° S (Walvis Bay area) in the Namibian upwelling system. Red stars stand for the FRS Africana (December 2009) data. Positive flux means an outgasing of $N_2O$ from the ocean to the atmosphere.





BGD
8, 3537–3618, 2011